DOKUZ EYLÜL UNIVERSITY

GRADUATE SCHOOL OF NATURAL AND APPLIED SCIENCE

INVESTIGATION OF THE PRODUCTION OF REFRACTORY METAL CONTAINING HIGH ENTROPY ALLOYS

by

Dilan UĞURLUER

September,2022

İZMİR

INVESTIGATION OF THE PRODUCTION OF REFRACTORY METAL CONTAINING HIGH ENTROPY ALLOYS

A Thesis Submitted to the
Graduate School of Natural and Applied Sciences of Dokuz Eylül University
In Partial Fulfillment of the Requirements for the Master of Science in
Metallurgical and Materials Engineering

by
Dilan UĞURLUER

September,2022
İZMİR

M.Sc THESIS EXAMINATION RESULT FORM

We have read the thesis entitled **"INVESTIGATION OF THE PRODUCTION OF REFRACTORY METAL CONTAINING HIGH ENTROPY ALLOYS"** completed by **DİLAN UĞURLUER** under supervision of **Asst. Prof. Dr. Murat ALKAN** and we certify that in our opinion it is fully adequate, in scope and in quality, as a thesis for the degree of Master of Science.

.....

Asst. Prof.Dr. Murat ALKAN

Supervisor

.....

Assoc. Prof.Dr. Mehmet BUĞDAYCI

Jury Member

.....

Assoc. Prof.Dr. Esra DOKUMACI ALKAN

Jury Member

Prof.Dr. Okan FISTIKOĞLU

Director

Graduate School of Natural and Applied Sciences

ACKNOWLEDGEMENTS

I would like to express my deep and sincere appreciation to my supervisor Asst. Prof. Dr. Murat ALKAN for his patience, guiding, support. I am grateful to Assoc. Prof. Dr. Esra Dokumacı ALKAN for her examination and guiding on the thesis.

I would like to thank my friend Aslıhan KARAKANAT for providing me with moral support and encouragement.

I would like to thank Research Assistants Orkut SANCAKOĞLU for his suggestions and increasing motivation, Ramazan DALMIŞ for his help in laboratory studies, and Saadet GÜLER for his support and friendship.

I would like to acknowledge the help provided by the technical staff in the Department of Metallurgical and Materials Engineering of Dokuz Eylül University.

TUBITAK supported this thesis in the scope of Project no 118M204. I am pleased to acknowledge MTA (General Directorate of Mineral Research and Exploration) for assistance in chemical analysis.

Most importantly, I express my thanks to my mother and father, Fatma UĞURLUER and, Mehmet Nuri UĞURLUER, and other family members for their all support and for preparing me for my future.

Dilan Uğurluer

INVESTIGATION OF THE PRODUCTION OF REFRACTORY METAL CONTAINING HIGH ENTROPY ALLOYS

ABSTRACT

In the present study, the production of $CrFeNiME_IME_{II}$ (ME = Mo, Nb, Ta, V, W) high entropy alloys containing refractory metals was carried out using self-propagating high-temperature synthesis (SHS) technique. The fourth and fifth elements constituting the HEA composition were selected among the refractory metals. Equiatomic alloys of CrFeNiMoNb, CrFeNiTaMo, CrFeNiNbV and CrFeNiVW have been produced.

The first series of thermodynamic analyses were realized to calculate the specific heat and adiabatic temperature values of the SHS reactions for the targeted alloys. The reduction experiments were carried out for the thermodynamically competent SHS reactions. The chemical, phase, and microstructure analyses of the obtained products were realized, and their mechanical properties were examined.

In the SHS experiments, aluminothermic and silicothermic reductions were performed. Different metal oxide powders (Fe_2O_3, Cr_2O_3, NiO, MoO_3, V_2O_5, Nb_2O_5, WO_3, Ta_2O_5) were utilized as raw materials, and aluminum and ferrosilicon powders were used as the reducing agents. The final products were characterized using XRF, XRD, SEM/EDS, and hardness tests. The metallic distributions on the products and metal recovery efficiencies were calculated depending on the chemical analyses. Among the refractory metals, the highest recovery efficiency was achieved in W and the lowest recovery efficiency in Ta.

Keywords: Microstructure, SHS, high entropy alloy

REFRAKTER METAL İÇERİKLİ YÜKSEK ENTROPİLİ ALAŞIMLARIN ÜRETİLMESİ VE GELİŞTİRİLMESİ

ÖZ

Bu çalışmada $CrFeNiME_IME_{II}$ (ME = Mo, Nb, Ta, V, W) refrakter metal içerikli yüksek entropili alaşımların üretimi kendiliğinden ilerleyen yüksek sıcaklık sentezi (SHS) yöntemi kullanılarak gerçekleştirilmiştir. Refrakter metaller arasından dördüncü ve beşinci elementler seçilmiştir. CrFeNiMoNb, CrFeNiTaMo, CrFeNiNbV ve CrFeNiVW alaşımları üretilmiştir.

Hedef alaşım sistemleri için gerekli termodinamik analizler yapıldıktan sonra SHS yönteminde kullanılan spesifik ısı ve adyabatik sıcaklık değerleri hesaplanmıştır. Uygun enerji değerleri elde edilip deneysel çalışmalar gerçekleştirilmiştir. Elde edilen ürünlerin kimyasal analizi, faz analizi, mikroyapı analizi yapılmış ve mekanik özellikleri incelenmiştir.

Deneysel çalışmalarda alüminotermik ve silikotermik indirgeme yapılmıştır. Hammadde olarak metal oksit tozları (Fe_2O_3, Cr_2O_3, NiO, MoO_3, V_2O_5, Nb_2O_5, WO_3, Ta_2O_5) ile indirgeyici olarak alüminyum ve ferrosilisyum tozları kullanılmıştır. Elde edilen nihai ürünler XRF, XRD, SEM/EDS ve sertlik testleri kullanılarak karakterize edilmiştir. Kimyasal bileşimleri belirlenen alaşım ve cüruflara elementel verim analizleri yapılmıştır. En yüksek refrakter metal verimi W elementinde, en düşük verim ise Ta elementinde görülmüştür.

Anahtar kelimeler: Mikroyapı, SHS, yüksek entropili alaşım

CONTENTS

Page

LIST OF FIGURES

Page

LIST OF TABLES

Page

CHAPTER 1
INTRODUCTION

Depending on human demands, alloy compositions have evolved from simple to complicate. Through the discovery of new alloys, progress has occurred in civilizations, and the performance of alloys has increased. Exceptional alloys like stainless steel, high-speed steel, and superalloys have been discovered in the last century. High entropy alloys have been acquired lately (Yeh, 2016).

High entropy alloys (HEAs) are defined as solid solution alloys containing at least five principal elements with variable compositions between 5 to 35 atomic percentages. Unlike conventional alloys, HEAs are composed of multi-principal elements. In HEAs, the mixing entropy will be maximum for a solution phase. As the mixing entropy increases, the number of phases in the alloys decreases. In this way, unique alloys with improved mechanical properties have been developed. High entropy alloys can be used in many applications because of their high potential. HEAs can exhibit excellent mechanical and magnetic properties and be used in nuclear industries, mobile applications, or thermal barrier coating. HEAs can also be used for ceramics, polymers, or traditional alloys as a coating (Y. Zhang et al., 2014).

The production of high entropy alloys plays an essential role in the evolution of the alloy world. In recent years, research for high entropy alloys has been continuously increasing. In this thesis, unlike the literature, High Entropy Alloys were produced by the Self-Propagating High-Temperature Synthesis method (SHS). The SHS method has some advantages. Since the SHS method is fast, environmentally friendly, low cost, and sustainable, producing high entropy alloys containing refractory metals with this method has been investigated. In this context, the mixtures of different metal oxide powders (Fe_2O_3, Cr_2O_3, NiO, MoO_3, V_2O_5, Nb_2O_5, WO_3, Ta_2O_5) were used as raw materials. Aluminum and ferrosilicon powders were used as the reducing agents. The starting mixtures were prepared to obtain the estimated CrFeNiMoNb, CrFeNiTaMo, CrFeNiNbV, and CrFeNiVW alloys in equiatomic compositions, and the final products were characterized.

CHAPTER 2
TEORICAL BACKGROUND

2.1 Entropy

Thermodynamics mainly focuses on the relationship between macroscopic features such as temperature, volume, mass density, and pressure. The second law of thermodynamics expresses that the overall entropy of the system and the surroundings enhances in any spontaneous process. Entropy is a thermodynamic function investigated in two different ways as chemical and statistical thermodynamics. Entropy is calculated by Eq (2.1) in chemical thermodynamics (Aytekin, 1993).

$$dS = \frac{\Delta Q}{T} \tag{2.1}$$

Where S is the entropy, Q is the heat flow, and T is the absolute temperature.

Entropy in statistical mechanics was enhanced by Ludwig Boltzmann in the 1870s. The statistical behavior of the microstates was investigated. Boltzmann remarked that the configurational entropy of a system is connected with the logarithm of the number, *w*, of microstates that compose the macrostates (Greven et al., 2003):

$$\Delta S_{conf} = k \ln w \tag{2.2}$$

Where k = 1.38 x 10^{-23} J/K is Boltzmann's constant. The total mixing entropy is the sum of the configurational, vibrational, magnetic dipole, and electronic randomness entropies. The relationship between them is shown in Eq. (2.3) (W. Zhang et al., 2018):

$$\Delta S_{mix} = \Delta S_{mix}^{conf} + \Delta S_{mix}^{vib} + \Delta S_{mix}^{elec} + \Delta S_{mix}^{mag} \tag{2.3}$$

The configurational entropy symbolizes the mixing entropy. Therefore calculations of the other three contributions are not regarded. In a solid solution that consists of an n-component, the configurational entropy per mole is calculated by Eq. (2.4), where R is the gas constant, x_i is the mole fraction of the i^{th} element, and n is the number of the components (W. Zhang et al., 2018):

$$\Delta S_{conf} = -R \sum_{i=1}^{n} X_i \ln X_i \quad (2.4)$$

According to the Richard's rule, the change of entropy per mole during the melting of metal almost equals one gas constant, R. Hence, R gas constant is used in the entropy definition of metallic alloy. The configurational entropy is reached its maximum for equiatomic alloys. As shown in Table 2.1, when the number of constituent elements increments, the ideal configurational entropy (equation 2.5) also increases in the same way (Yeh, 2016).

$$\Delta S_{conf} = -R \ln {}^{1}/_{n} = R \ln n \quad (2.5)$$

Table 2.1 Configurational entropies in R for equiatomic alloys (Yeh, 2016)

n	**1**	**2**	**3**	**4**	**5**	**6**	**7**	**8**	**9**	**10**	**11**	**12**	**13**
ΔS_{conf}	0	0.69	1.10	1.39	1.61	1.79	1.95	2.08	2.20	2.30	2.40	2.49	2.57

Materials are classified into three categories according to their configurational entropies:

Low entropy alloys (LEAs): $\Delta S_{conf} \leq 1R$,

Medium entropy alloys (MEAs): $1R \leq \Delta S_{conf} \leq 1.5R$,

High entropy alloys (HEAs): $\Delta S_{conf} \geq 1.5R$ (Murty, Ranganathan, et al., 2019).

The configurational entropies of traditional alloys are shown in Table 2.2. Table 2.2 shows that steels and copper alloys have a low entropy, and superalloys and bulk metallic glasses have medium entropy values (Murty, Ranganathan, et al., 2019).

Table 2.2 The configurational entropies of traditional alloys in a liquid state (Murty, Ranganathan, et al., 2019)

Systems	**Alloys**	**ΔS_{conf}**
Stainless steel	30	0.96 R (low)
Cu alloy	7-3 brass	0.61 R (low)
Ni-base superalloy	Inconel 718	1.31 R (medium)
Co-base superalloy	Stellite 6	1.13 R (medium)

2.2 High Entropy Alloys

High entropy alloys are promising new material groups. The concept of entropy has been emphasized so as to understand the high entropy alloys. The history, basic principles, application areas, HEA types, and physical metallurgy of high entropy alloys have been subsequently explained.

2.2.1 History of HEAs

The history of alloys goes back to 3000 B. C. and plays an enormous role in the survival and development of humanity. Bronze is the first alloy to influence human history. The Bronze Age began when humanity alloyed copper and tin. Many tools and weapons were made of bronze. Afterward, the Iron Age began, and many alloy groups were discovered (Murty et al., 2019). Figure 2.1 shows the historical evaluation of the materials with increasing entropy. From bronze, iron, and superalloys to Mg alloys, as the chemical composition increases, the configurational entropy of materials increases over time. Moreover, high entropy alloys were born in 2004 (Y. Zhang, 2019).

Jien-Wei Yeh and Brian Cantor issued two different studies in 2004, and S. Ranganathan also published another study in 2003. These publications have caused the formation of a new material group. These alloy groups are called high-entropy alloys. It is a new historic moment in the history of materials, and the number of publications has been increasing every year since 2004. In 1981, Cantor researched equiatomic high entropy alloys, one of which contains 20 components. Considering this research, it was found that $Co_{20}Cr_{20}Fe_{20}Mn_{20}Ni_{20}$ alloy system had only one FCC phase. It shows that five elements get mixed as a solid solution. In 1995, Jien-Wei Yeh produced 40 equiatomic alloy systems containing 59 elements using the arc melting technique. The microstructure, hardness, and corrosion resistance of alloys have been studied after casting and annealing. It was determined that the alloys had excellent corrosion resistance, and as-cast and annealed alloys have hardness values within the run of 590 to 890 HV (Yeh, 2016).

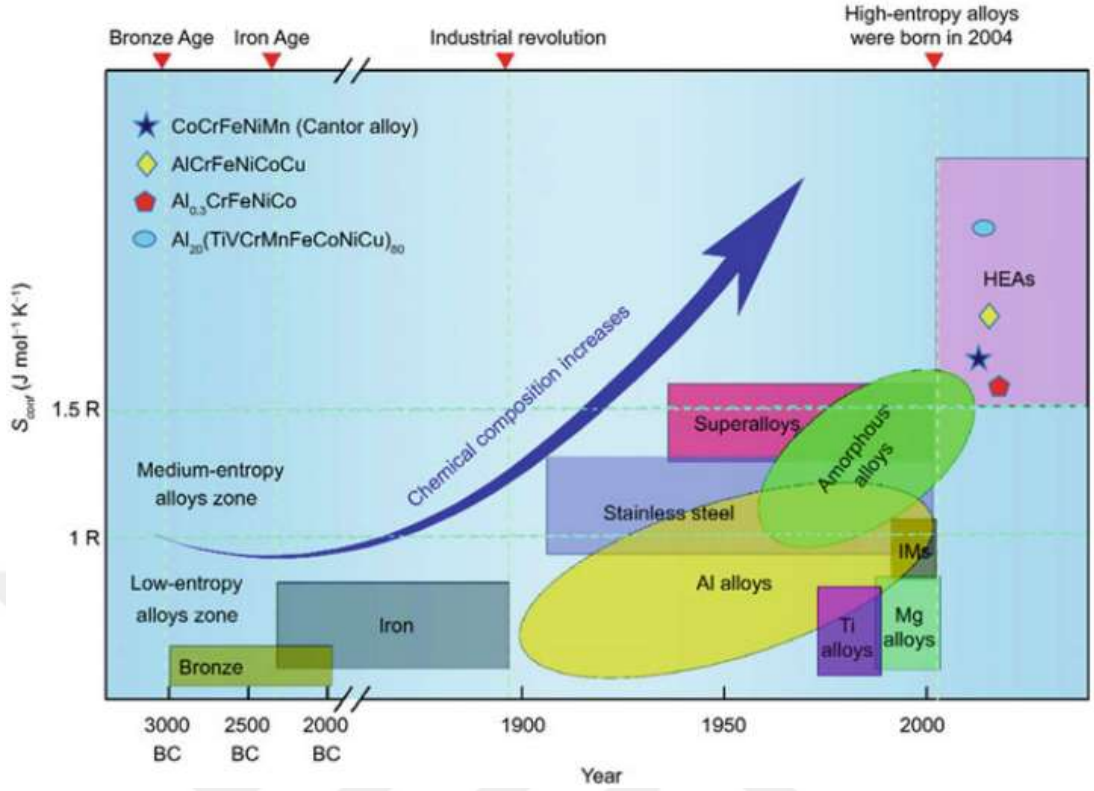

Figure 2.1 Historical evolution of the metallic materials (Y. Zhang, 2019)

2.2.2 Definition of HEAs

Two definitions based on entropy and composition are used to explain high entropy alloys. Considering that an alloy system, whether it contains a single phase or multiphase at room temperature, HEAs should have the configurational entropy larger than 1.5R according to the composition-based definition. The definition is expressed as follows (W. Zhang et al., 2018):

$$\Delta S_{conf} \geq 1.5R \tag{2.6}$$

HEAs are characterized as combinations containing at least five major elements, and each one has an atomic percentage (at.%) between 5 and 35. If there are any minor elements, the atomic percentage of each one should be smaller than five at.%. This definition is stated as takes after:

$$\begin{aligned} n_{major} &\geq 5, \quad 5 \text{ at. } \% \leq x_i \leq 35 \text{ at. } \% \\ n_{minor} &\geq 0, \quad x_j \leq 5 \text{ at. } \% \end{aligned} \tag{2.7}$$

Where $_{major}$ and $_{minor}$ are the numbers of major and minor elements, respectively, x_i and x_j are the atomic percentages of major element i and minor element j, respectively (W. Zhang et al., 2018).

2.2.3 Application areas of HEAs

Materials science has developed as long as the technical fields like energy, aerospace, and manufacturing have advanced. New materials are investigated with increasing demands like higher strength, wear resistance, and superior magnetic properties. Therefore, material selection has become more critical. The relationship between the structure, properties, and manufacturing/processing is examined to determine the application area. According to the research, high entropy alloys have met the expected properties and found many application areas due to unique properties (Davis, 1990).

High entropy alloys can be used in a wide run of applications as functional and structural materials. Some of the application areas of HEAs are as follows: functional coatings, tool materials with better strength, wear and oxidation resistance, lightweight, high-temperature materials, and nuclear industry materials (Yeh, 2006).

As regards previous studies, high entropy alloy systems can be used for a different purposes. CrMnFeCoNi alloy system can be utilized in cryogenic applications for liquefied gas storage with maintaining mechanical properties at low temperatures. HEAs are mainly used in coatings because of their higher strength, hardness, and corrosion resistance. They can be used in cutting tool steels, high-speed steels as hard coatings, or in food preservation as anti-oxidation and anti-corrosion materials (Chikumba & Rao, 2015).

2.2.4 Classification of HEAs

Many material groups have been developed using the high entropy effect recently. High entropy alloys are classified as high-entropy superalloys (HESAs), high-entropy refractory alloys (RHEAs), lightweight high entropy alloys (LWHEA), and

high-entropy bulk metallic glasses (HEBMGs). High entropy superalloys are the same as high entropy alloys because of containing many constituents, and the microstructures of HESAs are similar to superalloys. Hence, this sub-group is called high entropy superalloys (Tsai, 2016).

High-entropy refractory alloys, which consist of refractory elements, are used for high-temperature applications. Lightweight high entropy alloys are reported that have higher mechanical properties, unlike conventional light metals. These alloy systems contain low-density elements (e.g., Al, Mg, Ti, Si, V, Li, Ca, Sc). Bulk metallic glasses are similar to high entropy alloys since both have multiple elements, but HE-BMGs have very high strength and toughness (Tsai, 2016).

2.2.5 Physical Metallurgy

Their physical metallurgy affects the microstructure, physical and mechanical properties of high entropy alloys. Four core effects are used to understand their structure and properties: high entropy effect, sluggish diffusion effect, severe lattice distortion effect, and cocktail effect. The relationship between the four effects and their correlation in HEAs shows that the high entropy effect determines the microstructure and should be incorporated into thermodynamics. The sluggish diffusion effect is relevant to phase transformation. The severe lattice distortion has a broader impact. It affects structure, property, deformation mechanism, and also thermodynamics. The cocktail effect is a whole effect for high entropy alloys (Cheng et al., 2017).

Alloys containing many principal elements are thought to have fragile and complex microstructures because of forming intermetallics. Due to high configurational entropy, it has been observed that HEAs have solid solution phases. Unlike the expected, this effect reduces the number of phases and stabilizes solid solutions (Yeh, 2015).

The sluggish diffusion of elements plays an essential role in phase transformations. When comparing the diffusion coefficients of pure metals, stainless steel, and high entropy alloys, diffusion rates of these alloy systems are as follows: HEAs < stainless steels < pure metals (Y. Zhang et al., 2014).

HEAs have a low diffusion rate, so the phase transformation rate in the multielement matrix is lower. High entropy alloys accept as a soluble matrixThe diffusion of an atom in the solute matrix is tally unlike from diffusion in the matrix of traditional alloys (Yeh, 2015). Figure 2.2 shows the activation energies of pure elements and alloy systems. The sluggish diffusion effect is associated with the number of elements. CoCrFeMnNi alloy has the highest Q/T_m value, while the pure metals have the lowest (Yeh, 2013).

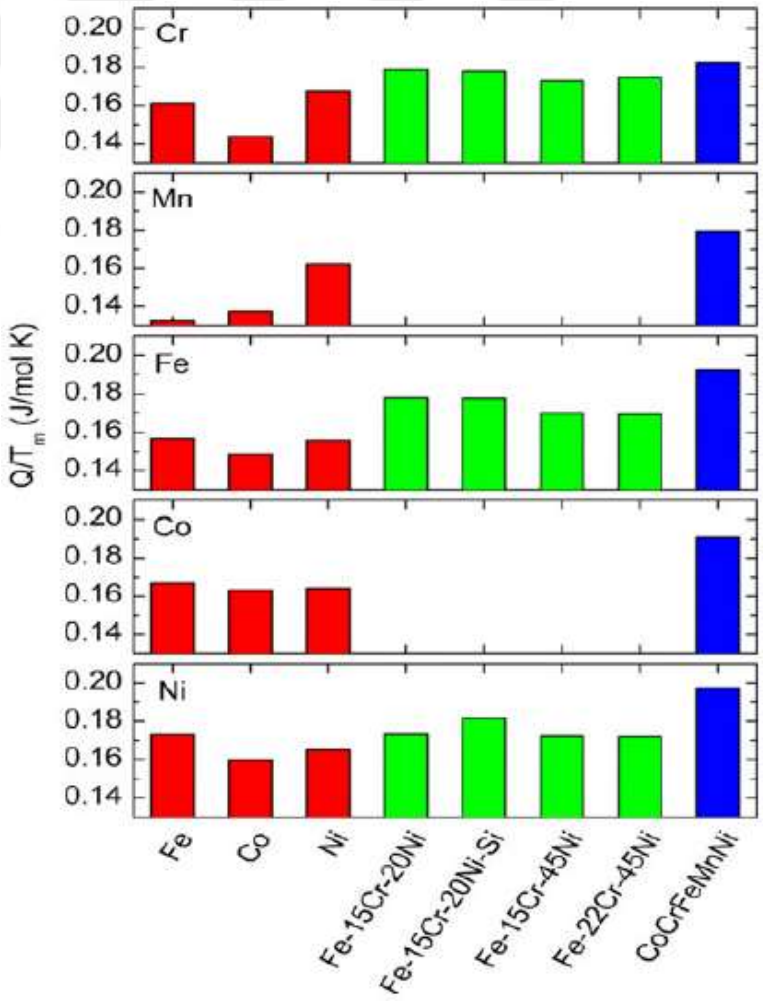

Figure 2.2 Q/T_m energies for Cr, Mn, Fe, Co, and Ni in different matrices (Yeh, 2013)

Severe lattice distortion happens since high entropy alloys comprise of elements with different atomic sizes in the solute matrix. It influences the properties of materials in mechanical, thermal, electrical, optical, and chemical. For instance, lattice distortion effects cause an increase in hardness and strength and also cause a decrease in electrical and thermal conductivities (Yeh, 2015). Figure 2.3 shows that a pure metal has the same type of atoms; hence there is no distortion in the lattice. In dilute alloys, the presence of different atoms causes mild distortion. Different atoms surround whole atoms with different atomic sizes in high entropy alloys so that the severe lattice distortion effect can be observed clearly (W. Li et al., 2021).

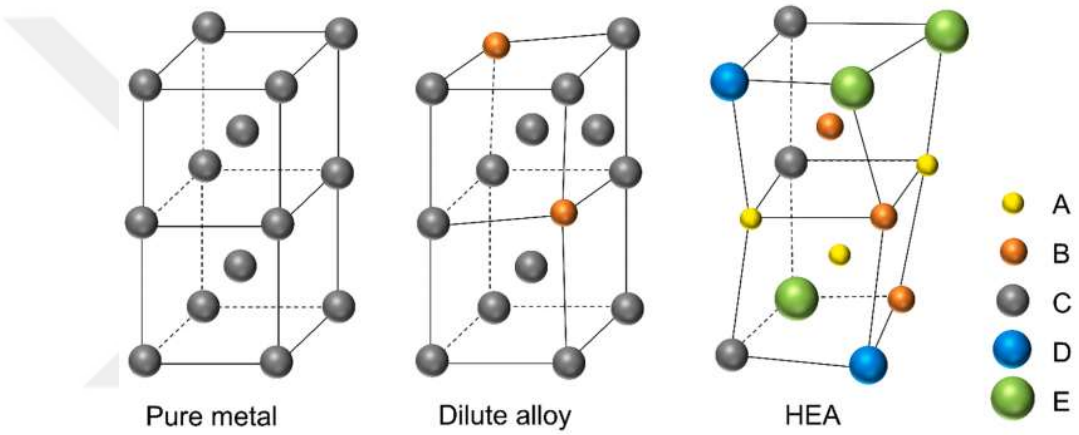

Figure 2.3 Distorted lattice in high entropy alloys (W. Li et al., 2021)

The cocktail effect is approximately the interaction between constituent elements and affects the composition, structure, and microstructure of the material. For instance, adding lightweight elements reduces the density of the alloy, while adding refractory elements increases the melting point (Cheng et al., 2017).

2.3 Synthesis And Processing

The preparation method of high entropy alloys can be classified into three groups based on the starting states: liquid, solid, and gas mixtures. Figure 2.4 shows the fabrication routes of HEAs. The solid-state metallurgy route contains mechanical alloying. The liquid metallurgy route includes arc melting, Bridgman solidification, laser melting, and laser cladding. Elements could be mixed from the vapor state in

another route, including sputter deposition, pulse-laser deposition (PLD), and atomic-layer deposition (ALD) (W. Zhang et al., 2018).

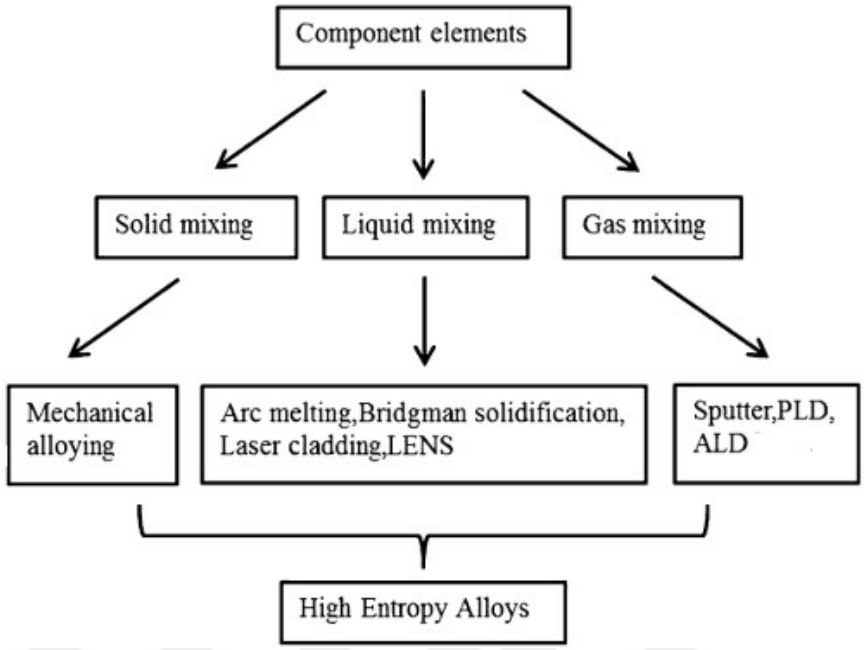

Figure 2.4 Fabrication routes of HEAs (Yeh, 2016)

2.3.1 Solid State Metallurgy Route

Mechanical alloying (MA) is a solid-state powder process in a high-energy ball mill to obtain homogeneous alloy. This technique was evolved to manufacture oxide-dispersion-strengthened Ni-base and Fe-base superalloys by Benjamin. MA is suitable for producing several alloys like amorphous alloys, intermetallics, and aerospace components (Murty, Yeh, et al., 2019). Mechanical alloying is carried out at room temperature or below. Hence, alloys could be produced with very different melting temperatures by this method. It also prevents segregation and other problems based on melting and casting methods (Yeh, 2016).

In this method, raw materials are mixed in a ball mill and ground into fine powders. A hot-isostatic-pressing (HIP) process is applied to compress and sinter the powders. In order to remove internal stresses, a heat-treatment process is then applied

as a final step. Figure 2.5 indicates the schematical illustration of the mechanical alloying (Y. Zhang et al., 2014).

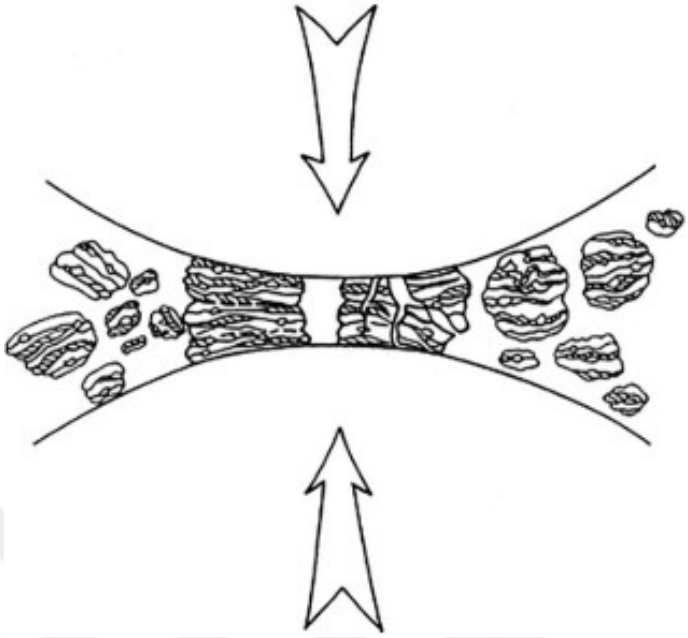

Figure 2.5 Schematic representation of mechanical alloying (Y. Zhang et al., 2014)

2.3.2 Liquid Metallurgy Route

2.3.2.1 Arc Melting

Arc melting is the foremost preferred method for producing high entropy alloys. High temperatures (>3000 °C) are reached in the arc melting furnace and can be checked by electrical power. However, low-melting elements could be evaporated at high temperatures, and the composition of the alloy system could not control. Hence, induction heating could be a better choice (Y. Zhang et al., 2014). A schematic view of the vacuum arc furnace is shown in Figure 2.6.

All components are first blended within the liquid state and after that solidified within copper crucible. In order to achieve homogeneity in the microstructure of alloys, numerous melting and solidification processes are used. The shape of the final product is button-like (Yeh, 2016).

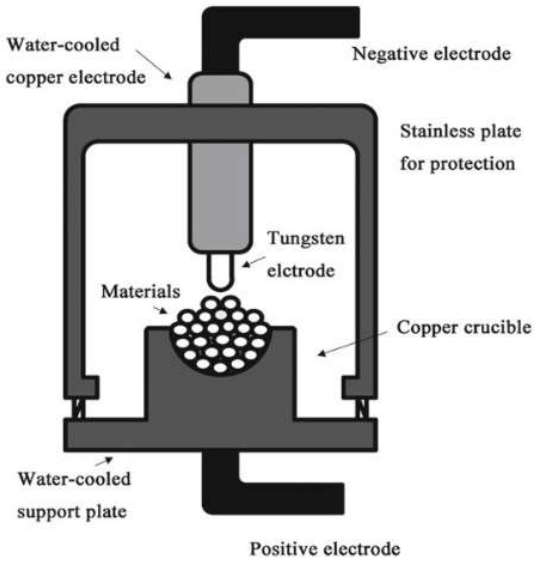

Figure 2.6 Schematic view of the vacuum arc furnace (Y. Zhang, 2019)

2.3.2.2 Bridgman Solidification Casting

Bridgman solidification is also called the Bridgman–Stockbarger method. Bridgman solidification technique (BST) could be utilized for microstructure control and property optimization and also to obtain single-crystal ingots. In this technique, the polycrystalline material is heated above its melting temperature and then cooled slowly. A single crystal structure with the same crystallographic order as the seed material begins to form and grow along the crucible. This process could be applied in horizontal or vertical directions (Y. Zhang et al., 2014).

In order to produce an alloy via BST, the materials are filled in a crucible and melted by inductive or resistant heating. The melted alloys are gradually pulled down to the low-temperature zone. The crystal grows at the solid-liquid interface and cools in a controlled (Y. Zhang et al., 2014).

2.3.2.3 Laser Melting and Laser Cladding

In the laser cladding method, intense beam energy from the laser is used as a heat source. The heat-affected area on material surface is much smaller. Thus, the formation of cracking, voids, and deformation are be decreased. A laser cladding system involves a laser source, optics, feeder, and manipulator. The optics and laser stay steady, but the specimens move according to the laser. Synchronous feeding is

applied to cladding materials and then solidified. This method is suitable for applying to products of various sizes and shapes (Yeh, 2016).

Laser cladding was generally focused on the coatings of Ni- and Co-based alloys until today. Due to the features such as high strength, hardness, and high oxidation resistance provided by high entropy alloys, various HEAs have been produced by the laser cladding method (Yeh, 2016).

2.3.3 Gas Mixing

2.3.3.1 Sputtering Deposition

The most common technique for producing high entropy alloy films is magnetron sputtering deposition. Atoms are repulsed from sputtering target depending on ion or atom shelling from sputtering gas. The substrate generates a random distribution of these sputtered atoms (Yeh, 2016).

2.3.3.2 Pulsed Laser Deposition (PLD)

Pulsed laser deposition (PLD) is an effective method for depositing materials with complex stoichiometry. A powerful laser beam from vacuum chamber hits the rotary high entropy alloy object. Due to overheating, atoms, ions, and electrons evaporate from the target material, and these are in the form of a plasma plume on the substrate surface as a thin film (Yeh, 2016).

2.3.3.3 Atomic Layer Deposition (ALD)

Atomic layer deposition (ALD) is another thin film deposition process used to control atomic layer and film growth of deposited material. ALD can generate reasonable surfaces with high delicate at an atomic dial. Therefore, it could be a manufacture strategy that gives extraordinary points of interest in thin film technology (Yeh, 2016).

Two chemicals called precursors are used in ALD reactions. The precursors react sequentially with the material's surface so that all reactions are carried out at the

surface. When successive exposure to different precursors, the thin film is slowly deposited. After all, surfaces are covered with an atomic layer, the reaction stops (Yeh, 2016).

2.4 SHS

Self-propagating high-temperature synthesis (SHS) is a production method of materials. SHS, also known as combustion synthesis, fabricates high-quality ceramics and refractory compounds. This process is very similar to thermite reactions. As a start, ignition of the process is performed. The exothermic reaction starts, and production occurs with the combustion wave's progression (Crider, 1982).

2.4.1 History of SHS

The history of SHS is connected with solid flame. In the 1960s, the effect of gasification on combustion was investigated. In one of the studies, gasless iron-aluminum thermite diluted with alumina was prepared. Since reactants and products are kept in a condensed state, the initial weight of the sample is retained. Investigation of gasless systems caused the discovery of solid flame (SF). SF is solid state combustion in which the reactants and products are solid even at high temperatures and can be used to obtain refractory materials. This method was called Self-propagating High-temperature Synthesis (SHS) (A. G. Merzhanov, 1995).

The SHS method was discovered in 1967 by Merzhanov and coworkers. After the fundamentals of SHS were determined, the product groups that can be produced with SHS were increased. Then, SHS technology was developed, and SHS materials were improved (A. G. Merzhanov, 1995).

2.4.2 SHS

Self-propagating high-temperature synthesis (SHS) is a simple and economical method for producing high-temperature materials and inorganic and organic

compounds. In this method, an exothermic reaction occurs with the spontaneous propagation of the combustion wave on the starting powder mixture in a single processing step, and the final product is obtained (Mishra & Pathak, 2009). Figure 2.7 shows the pattern of solid flame combustion.

Figure 2.7 Demonstration of the SHS method (Alexander G. Merzhanov, 2012)

SHS technique has several advantages and disadvantages. There is no need for high-temperature furnaces; hence the equipment cost is lower. Products with high purity requirements can be produced. Energy consumption is reduced. Processing time is much shorter than other methods; rapid production occurs. Despite these advantages, several limitations can be seen. SHS is an explosive method; thus, precautions must be taken. SHS reactions cannot be controlled easily because the reaction takes a very short time to start and complete (Mishra & Pathak, 2009).

There are four essential temperatures in combustion synthesis: T_0, T_{ig}, T_{ad}, and T_c. Initial temperature (T_0) is the average temperature of whole reactant powders before the ignition occurs. Ignition temperature (T_{ig}) is the temperature at which reagent starts. Adiabatic temperature (T_{ad}) is the highest temperature reached under adiabatic conditions. Actual combustion temperature (T_c) is the most elevated temperature come to beneath non-adiabatic conditions. Whereas T_0, T_{ig}, and T_c are generally measured during SHS reaction, T_{ad} is calculated by thermodynamic equations. T_{ad} must be higher than 1800K for an SHS process to occur (Pacheco, 2007).

The adiabatic temperature and the released energy during the reaction are two important thermodynamical parameters for metallothermic reduction. T_{ad} value is

used to understand whether 16the combustion wave can propagate spontaneously on the reactants and must be higher than 1800K (1527 °C) for an SHS process to 16occur. The released energy is another parameter known as the specific heat used to separate metal-slag in the products easily. The released energy during the reaction is calculated by dividing the formation enthalpy at 298 K by total weight of products. This value must be between 2250 J/g and 4500 J/g for the reaction to be controlled (Alkan, 2014).

$$T_{ad} \geq 1527\ °C,\ 4500\ J/g \geq \text{Released Energy} \geq 2250\ J/g \qquad (2.8)$$

Various material groups can be produced by the SHS technique. Self-propagating high-temperature synthesis is used to fabricate intermetallics, structural ceramics, hard alloys, powdered composites, and coatings (Borovinskaya, 1992). High entropy alloys can also be produced by this method, according to recent studies.

Sanin et al. used the SHS method for the first time in producing high entropy alloy systems. In this study, it is aimed to produce $NiCrCoFeMnAl_X$ (X = 0.2, 0.6, 1.0, 1.2, 1.6, 2.0) high entropy alloy. Metal oxide powder mixtures (NiO, Cr_2O_3, Co_3O_4, Fe_2O_3, MnO_2) and reducing metal powders (Al) were used as raw materials. The effect of Al addition to $NiCrCoFeMnAl_x$ high entropy alloy on density and hardness was investigated. According to their results, density and hardness values of the alloy systems increased with the increase in Al concentration in the alloy. The formation of the intermetallic phase can explain the increase in the hardness value. According to X-ray diffraction (XRD) data, at low concentrations (X = 0.2), a single-phase alloy system consisting of a solid solution with FCC structure was obtained. The alloy systems with three phases, BCC, FCC solid solutions, and β phase (NiAl intermetallic phase), were obtained at concentrations of $0.6 \leq X \leq 1.2$. The final alloy, composed of BCC solid solution and NiAl intermetallic phase, was obtained at $X \geq 1.6$ (Sanin et al., 2016).

CHAPTER 3
LITERATURE REVIEWS

3.1 High Entropy Superalloys

Stepanov et al. produced alloy systems with a duplex ultrafine-grained (UFG) structure using the SHS method to enhance tensile properties of high entropy alloys. CoCrFeNiMn alloy system including considerable quantities of Al and C (graphite powder) has been studied. As-cast alloys had one FCC phase structure with minor $M_{23}C_6$ carbide. CoCrFeNiMn alloys were cold-rolled and then annealed. After cold rolling and annealing, the carbides with small grain size increased, the B2 phase was formed, and the FCC structure recrystallized. Thus, an alloy system with duplex ultrafine-grained (UFG) structure was produced, and it was observed that improvements were made in its mechanical properties. The annealed alloy at 900 °C had a yield strength of 785 MPa, a tensile strength of 985 MPa, and an elongation of 32% (Stepanov et al., 2018).

Munitz et al. studied the $Al_{1.25}$CoCrCuFeNi alloy system produced by arc melting. The effects of heat treatment and cooling rate on structure were characterized. Heat treatments were applied between 650 and 850°C and induced the disordered BCC lamellar to change into the σ phase together with the FCC structures. Then alloy was reheated to 1040 °C, the σ phase turned into the disordered BCC, and the different FCC structure was nucleated. Fine-grained structures turned into coarse grains at 1200°C based on the heat treatment temperature in the regions of dendrite cores (Munitz et al., 2018).

Cui et al. investigated the microstructure and mechanical properties of $CoFeMnNiTi_x$ (x= 0.0- 0.25- 0.50- 0.75) alloys. Alloy systems were produced by the arc melting method. According to the XRD results, CoFeMnNi and $CoFeMnNiTi_{0.25}$ alloy systems contained single FCC phase, whereas $CoFeMnNiTi_{0.5}$ and $CoFeMnNiTi_{0.75}$ alloy systems contained FCC and Laves phases. The Laves phase, which possessed a hexagonal C14 structure, was defined as the Fe_2Ti type. For

$CoFeMnNiTi_x$ alloy systems, ductility decreased while strength increased with increasing Ti content. The hardness value increased from 136 HV to 583 HV. It was observed that the hardness of Laves structure was nearly twice that of the FCC phase. The elastic modulus of Laves structure is superior to the elastic modulus of the FCC phase in the existing alloy (Cui et al., 2018).

3.2 High Entropy Refractory Alloys

The first study on refractory high entropy alloys was published by Senkov et al. In this study, WNbMoTa and WNbMoTaV alloy systems were fabricated by vacuum arc melting. The hardness values were measured as 4455 MPa and 5250 MPa, respectively. High hardness values are due to solid solution hardening. Although both alloy systems enclose numerous components, it has been observed that there is only one BCC phase in the structure. According to BSE and EDS analysis, Ta exhibited a homogeneous distribution. Elemental mapping analysis is given in Fig. 3.1. W content was higher in dendrite arms, but V and Nb were low. According to the difference between the direct melting temperatures of the components and the melting temperature of the alloy, microsegregation has occurred (Senkov et al., 2010).

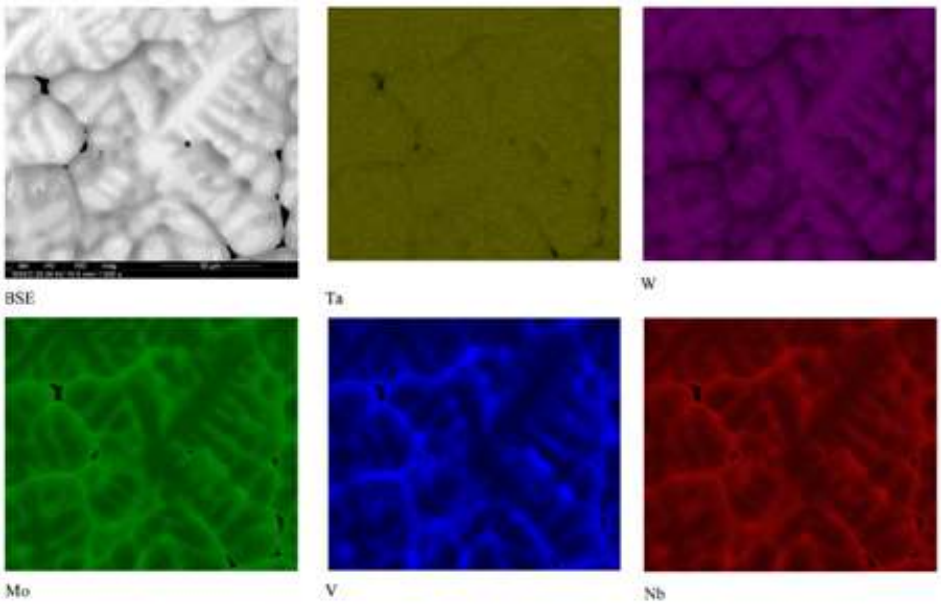

Figure 3.1 Elemental mapping analysis for WNbMoTaV alloy (Senkov et al., 2010)

Liu et. al studied the effect of Nb element on $CoCrFeNiNb_x$ (x = 0, 0.103, 0.155, 0.206, 0.309 and 0.412) alloy by using arc melting. Tensile tests were carried out at room temperature to research the effects on mechanical properties. The stress-strain (δ-ε) curves of high entropy alloys containing different amounts of Nb are shown in Figure 3.2. Tensile and yield strengths increased with Nb concentration. Nb_0 alloy possessed 413 and 147 MPa of the fracture and yield strengths, respectively. However, these values increased to 1004 and 637 MPa in the $Nb_{0.412}$ alloy. The tensile elongation decreased from 49.1% for the Nb_0 alloy to 1.3% for the $Nb_{0.412}$ alloy (Liu et al., 2015).

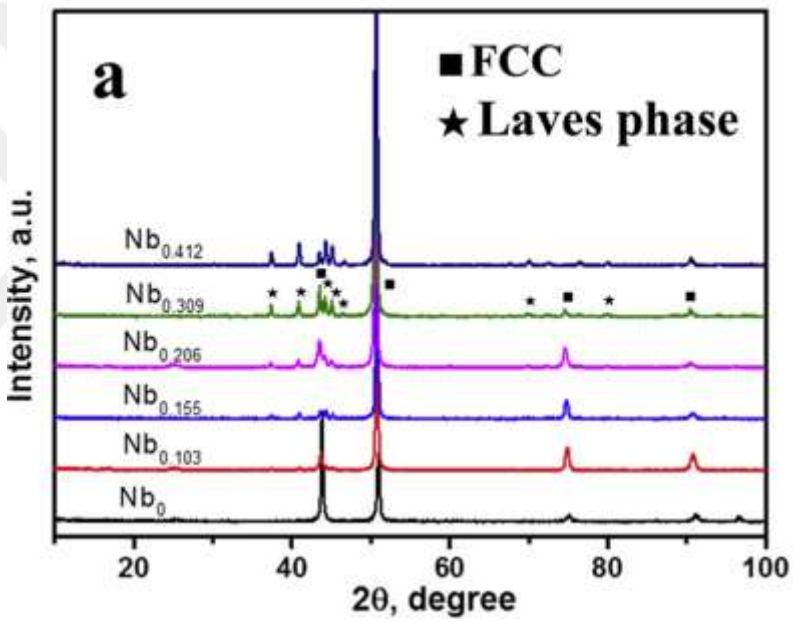

Figure 3.2 XRD patterns of $CoCrFeNiNb_x$ (x = 0, 0.103, 0.155, 0.206, 0.309 and 0.412) HEA (Liu et al., 2015)

Saikumaran et al. studied the microstructure of the CrFeMoV alloy system. The vacuum arc melting method was used for the production of equiatomic CrFeMoV. Dendritic microstructure with a high amount of Mo was seen due to the higher melting point of Mo. Thermodynamic phase analysis showed the existence of one BCC phase in the structure; however, there were two BCC solid solutions in CrFeMoV alloy due to the segregation of Mo to dendrites and Fe to interdendrites. Dendritic microstructure and the existence of columnar grain structure are shown in

Fig. 3.3(a,b). The distinction of composition among dendrites and interdendrites is shown in Fig. 3.3(c,d) (Saikumaran, Jaiganesh, et al., 2019).

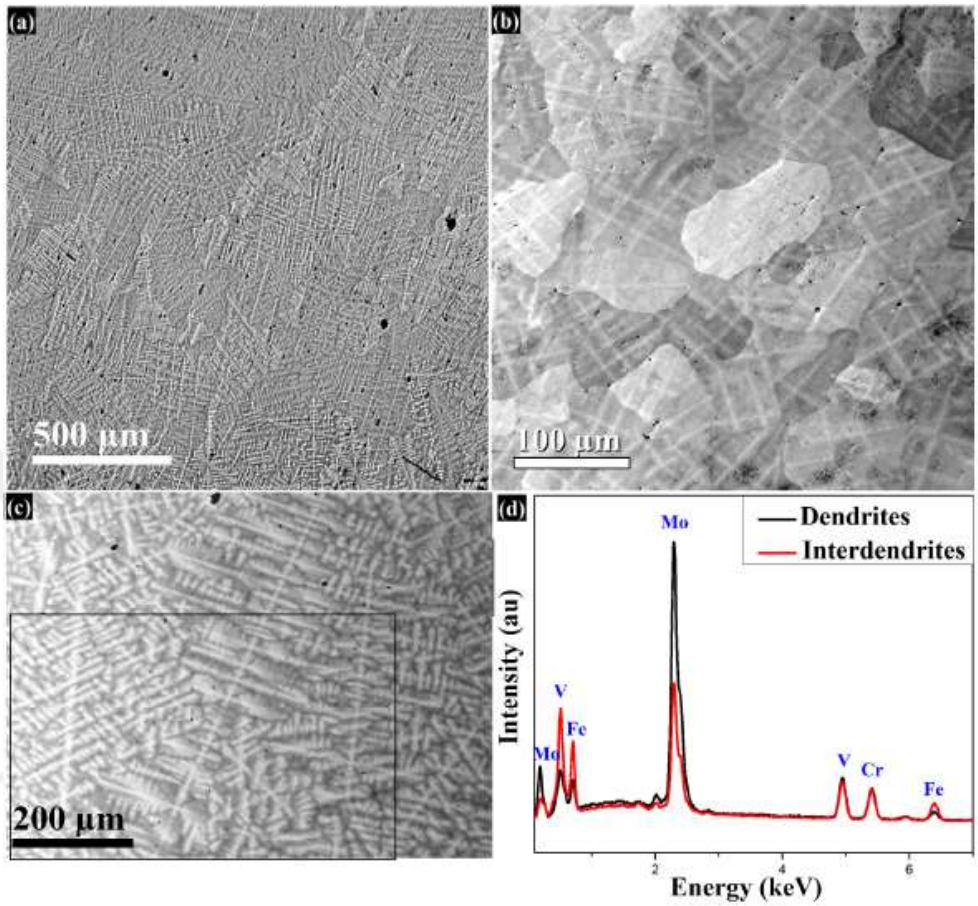

Figure 3.3 Microstructure analysis of CrFeMoV alloy(a, b, c) , EDX analysis (d) (Saikumaran, Jaiganesh, et al., 2019)

Saikumaran et al. studied the structure of CrFeNbNiV alloy produced by vacuum arc melting. Annealing was applied from 873 K through 1373 K, and the final products were investigated. There is no difference between aged conditions and as-cast alloy in microstructure and hardness. As-cast CrFeNbNiV alloy had a hardness of 1500 Hv. XRD analysis of CrFeNbNiV is given in Figure 3.4. CrFeNbNiV possessed a Nb rich NbCrNi type HCP Laves phase, two minor tetragonal and BCC phases. One of the tetragonal phases was defined as $V_{0.7}Ni_{0.3}$ type intermetallic phase. It is clear that Laves phase is a major phase, and the alloy system has various phases (Saikumaran, Mythili, et al., 2019).

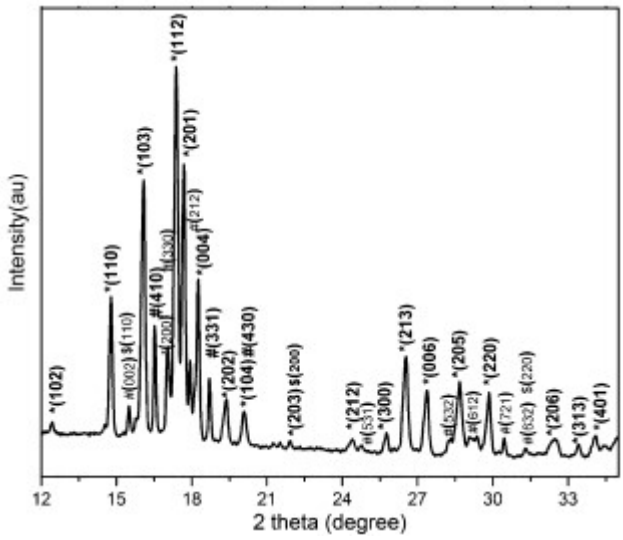

Figure 3.4 XRD pattern of CrFeNbNiV (Saikumaran, Mythili, et al., 2019)

Oleg Sobol investigated the characteristics and microstructure of high entropy alloys containing refractory metals. NbZr(ME_I, ME_{II}, ME_{III}) (ME = Ti, V, Zr, Ta, Hf) alloy systems were produced using vacuum arc melting method. As a result of the studies, Nb and Zr-based high entropy alloy consisted of a single-phase solution with a BCC crystal lattice. Nb element stabilized the BCC microstructure. It has been concluded that Nb-based alloys were composed of BCC, Zr-based alloys were HCP, and alloys using Zr and Nb as two basic elements consisted of a phase with BCC lattice structure (Sobol, 2020).

Kang et al. studied the microstructure of $Al_xCrNbVMo$ (x = 0.0, 0.5, and 1.0) refractory high-entropy alloys produced by powder metallurgy (PM). When Al was added to the alloy, elastic modulus decreased, and the density of CrNbVMo decreased below 8.0 g/cm^3 since Al has a lower elastic modulus and density. These alloy systems showed better mechanical properties than those produced before. CrNbVMo possessed 2743 MPa of the yield strength at room temperature and 1513 MPa of the yield strength at 1000°C. The yield strength of the CrNbVMo RHEA was enhanced by 27% at 25 °C and 87% at 1000 °C. Figure 3.5 shows the specific yield strength of AlxCrNbVMo alloy systems at different temperatures than other BCC RHEA's. Segregation was not observed in the microstructure, and there was only one BCC phase inhomogeneous structure (Kang et al., 2021).

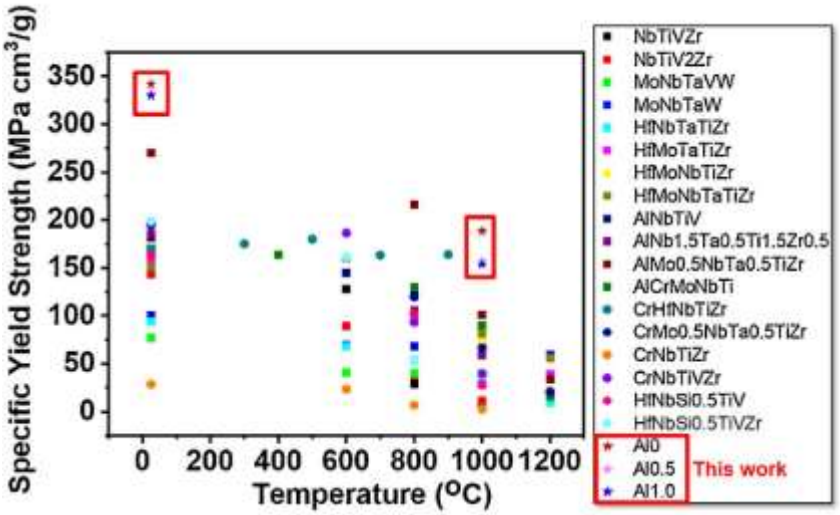

Figure 3.5 Yield strength of BCC RHEAs at different temperatures (Kang et al., 2021)

3.3 Light Weight High Entropy Alloys

Feng et al. studied the design of lightweight high entropy alloys identified as alloys with a density of less than 7.00 gcm^{-3}. Their microstructure is composed of solid solutions and intermetallics. Some elements are caused to the formation of very stable intermetallic compounds such as Al and Ti. Nevertheless, they have higher strength and hardness. Due to their unique physical and mechanical properties, lightweight HEAs are considered potential structural materials for transportation and defense industries (Feng et al., 2016).

Tseng et al. studied a lightweight HEA $Al_{20}Be_{20}Fe_{10}Si_{15}Ti_{35}$ produced by vacuum arc melting. The density of the alloy was 3.91 gcm^{-3}. The hardness of the alloy was 911 Vickers which is higher than Ti6Al4V and other lightweight HEAs such as AlNbTiVZr and AlLiMgZnSn. Furthermore, alloy consisted of one major solid solution and two minor phases. The composition of two minor phases includes Al_2(Ti, Fe) and Ti_5Si_3 (Tseng et al., 2017).

Li et al. studied the microstructure and mechanical properties of new lightweight HEAs. $Mg_X(MnAlZnCu)_{100-X}$ (X = 20, 33, 43, 45.6, 50) systems were prepared by induction melting. It has been observed that they have a density ranging from 2.20

gcm^{-3} to 4.29 gcm^{-3}, hardness of 178 - 429 HV, and high compression strength of 400- 500 MPa at room temperature. The microstructure had two phases: HCP and Al-Mn icosahedral quasicrystal phases (R. Li et al., 2010).

3.4 High Entropy Bulk Metallic Glasses

Bulk metallic glasses (BMGs) are generally based on a single principal element. However, high entropy bulk metallic glasses are included multiple major elements, unlike BMGs, and have remarkable mechanical properties (X. Q. Gao et al., 2011).

Bizhanova et al. studied the production of $Zr_{31}Ti_{27}Be_{26}Cu_{10}M_6$ (M=Ag, Al, Ni, V, Cr, Fe) and $Zr_{28}Ti_{24}Be_{23}Cu_9Ni_{10}N_6$ (N=V, Cr, Fe, Ag, Al) alloys by using arc melting. These high entropy bulk metallic glasses had high specific strength and compressive plasticity. The quinary alloys had better plasticity than senary alloys. However, the senary alloys possed higher strength. It has been observed that glass-forming ability was higher in $Zr_{31}Ti_{27}Be_{26}Cu_{10}Ni_6$, $Zr_{31}Ti_{27}Be_{26}Cu_{10}V_6$, and $Zr_{31}Ti_{27}Be_{26}Cu_{10}Ag_6$ systems (Bizhanova et al., 2018).

Li et al. studied new FeNiCrMo (P, C, B) high-entropy bulk metallic glasses prepared by induction melting. XRD patterns showed that $Fe_{55-x}Ni_{20}Cr_XMo_5(NM)_{20}$ (X = 20, 25, 30) and $Fe_{35-Y}Ni_{20}Cr_{25}Mo_Y(NM)_{20}$ (Y = 10, 15) had full glassy structure. These HEBMGs, which could be used as structural or coating materials, had a strength of 3.4 GPa and hardness of 1107 Vickers and showed excellent corrosion resistance in acids and NaCl solutions (Y. Li et al., 2020).

CHAPTER 4
EXPERIMENTAL STUDY

In this study, the target alloy systems were chosen as equiatomic $CrFeNiME_IME_{II}$ (ME = Mo, Nb, V, W) based refractory high entropy alloys. Self-propagating high-temperature synthesis (SHS) method was used during the production of refractory HEAs. This study is classified into three main titles: thermodynamic investigations, SHS experiments, and characterization studies. The flowchart of the study is given in Figure 4.1.

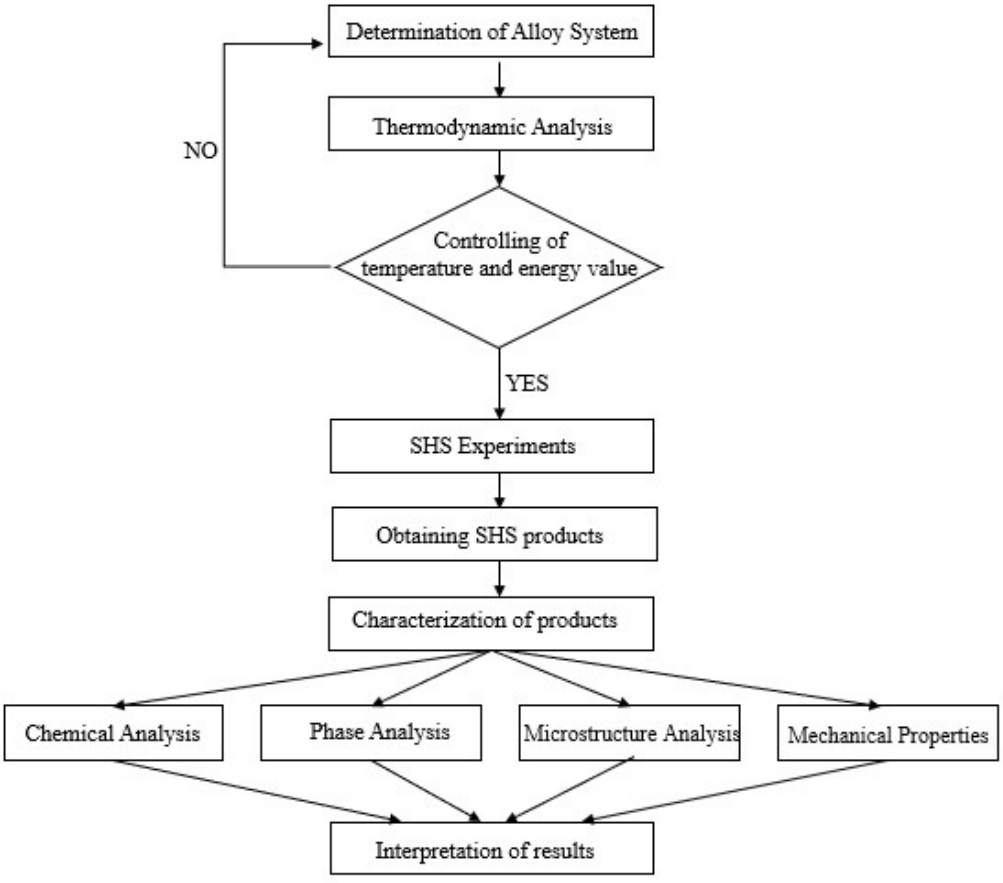

Figure 4.1 Flowchart of the experimental studies

4.1 Thermodynamic Analysis

HSC Chemistry 6.2, FactSage 7.3, and Thermo-Calc software with related databases were used to conduct thermodynamic studies after the target alloy

compositions were selected. The Gibbs free energy, the enthalpy, the adiabatic temperature, and the specific heat values of the reactions were calculated using the "Reaction Equations" and "Heat and Material Balances" modules in HSC Chemistry 6.2 software. Moreover, the possible phase compositions produced from cooling were calculated using the "Reaction" and "Equilib" modules in FactSage 7.3 and Thermo-Calc software.

4.2 Raw Materials

$CrFeNiME_IME_{II}$-based HEAs were the target alloys. ME_I and ME_{II} were selected between the refractory metals Mo, Nb, Ta, V, W. Four target alloys were selected: CrFeNiMoNb, CrFeNiTaMo, CrFeNiNbV and CrFeNiVW. Two different reducing agents were used: aluminum and ferrosilicon. Metal oxide powders such as Fe_2O_3, Cr_2O_3, NiO, MoO_3, V_2O_5, Nb_2O_5, WO_3, and Ta_2O_5 were used as the metal source in the raw mixtures. The average particle sizes of metal oxide powders are 75 – 150 μm and have a purity of at least 98%. Target alloy systems were produced using a reducing agent mixture. The mixture contains 25% stoichiometric ferrosilicon and 75% stoichiometric aluminum by weight. Ferrosilicon powders were obtained from Aveks İç ve Dış Ticaret, and aluminum metal powders were obtained from Cukurova Kimya Endüstrisi A.Ş. The main chemical reaction of the target refractory high entropy alloys, which are equimolar, is given below:

$$½Cr_2O_3+½Fe_2O_3+NiO+ME_IO_x+ME_{II}O_x+v_1Al+v_2Fe\text{-}Si=CrFeNiME_IME_{II}+y_1Al_2O_3+y_2SiO_2 \quad (4.1)$$

4.3 Method

SHS experiments were carried out under atmospheric conditions in Dokuz Eylül University, Faculty of Engineering, Metallurgical and Materials Engineering, casting laboratory. Metal oxide powders were kept in the drying oven at 100 °C for at least 2 hours to remove the moisture inside. The raw material powder mixture, calculated as 150 g in total, was weighed on precision scales. The raw material powder amounts are given in Table 4.1. The raw material mixture was placed in a plastic box and mixed in an Emor brand powder mixer at 600 rpm for 15 minutes. Then, the raw

mixture was fed into a copper crucible with an inner diameter of 60 mm and a height of 200 mm. $Cr_{25}Al_5$ alloy resistance wire having a 0.80 mm diameter was placed on the surface of the raw mixture, and a lid was used to cover the crucible. SHS reactions were initiated by applying a maximum power of 40 volts and 30 amps over the resistor wire. After SHS reactions were completed, metal and slag were obtained by rapidly cooling the crucible in water. The resulting products were characterized.

4.4 Characterization Studies

Chemical analysis, phase analysis, microstructure analysis, and mechanical properties were investigated in characterization studies. X-ray fluorescence (OLYMPUS Innov-X Delta DP-6000 XRF Analyzer) device was used for the chemical analysis of the obtained alloys and slags. The phase compositions of the SHS products were characterized by X-ray diffractometer (Rigaku D-Max 2200-PC, Cu Kα radiation) equipment. The microstructures of the products were characterized by a scanning electron microscope (SEM, JOEL JSM-6060) with EDS (Energy Dispersive Spectrometer). For microstructure analysis, the samples were ground by 80, 240, 400, 800, and 1200 grit sandpaper, respectively, and polished. The grinding and polishing process was carried out with PRESI MECAPOL P 230 Grinding – Polishing device. In the polishing process, a water-based size of 3 microns single crystal diamond paste supplied by Metkon Company was used. Shimadzu HMV-2 microhardness (micro-Vickers) device was used to analyze mechanical properties. Five Vickers hardness values were recorded by applying a 0.3 kg load to the samples. The average of these values was taken, and the standard deviation values were calculated.

CHAPTER 5
RESULTS and DISCUSSIONS

5.1 Results and Discussions of Thermodynamic Studies

The Gibbs Standard Free Energy value measures the stability of a metal oxide. At a specified temperature, as the free energy of formation of the metal oxide increases toward negative values, the stability of the metal oxide will increase. The Gibbs free energy changes of metal oxides at varying temperatures under one mole of oxygen gas are shown with the Ellingham Diagram (Figure 5.1).

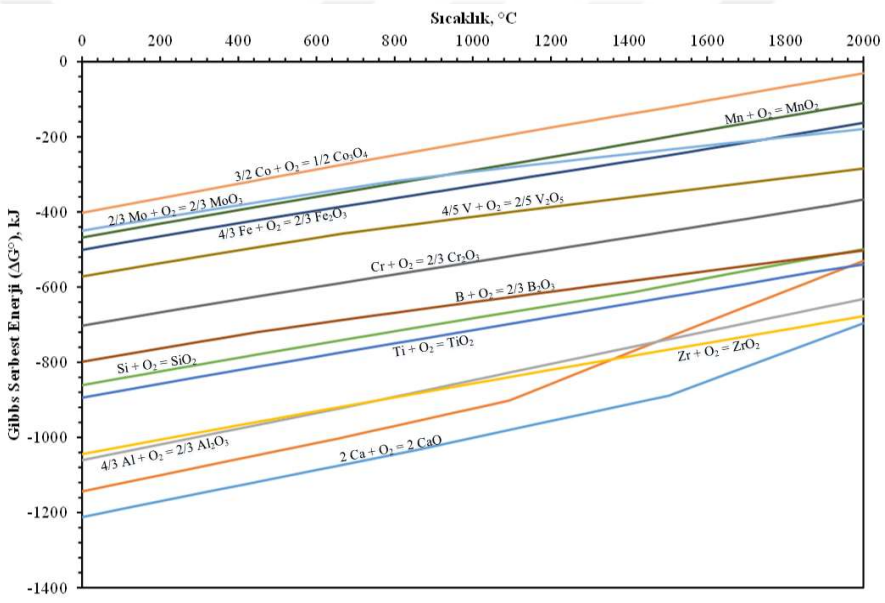

Figure 5.1. Ellingham Diagram is drawn with FactSage 6.3 software (Alkan, 2014)

Metallothermic reduction of a metal compound occurs when the metal used as a reducer has a higher affinity for the metal to be reduced than the non-metal compound such as halide, sulfur, and oxygen. For example, aluminum has a high affinity for oxygen, and as the differences in oxygen affinities between Al and another metal increase, it becomes easier to reduce the metal oxide with Al (Alkan, 2014). The Gibbs standard free energy change values measured as a result of the reduction of various metal oxides with Al and Si are given in Figure 5.2 and Figure 5.3, respectively.

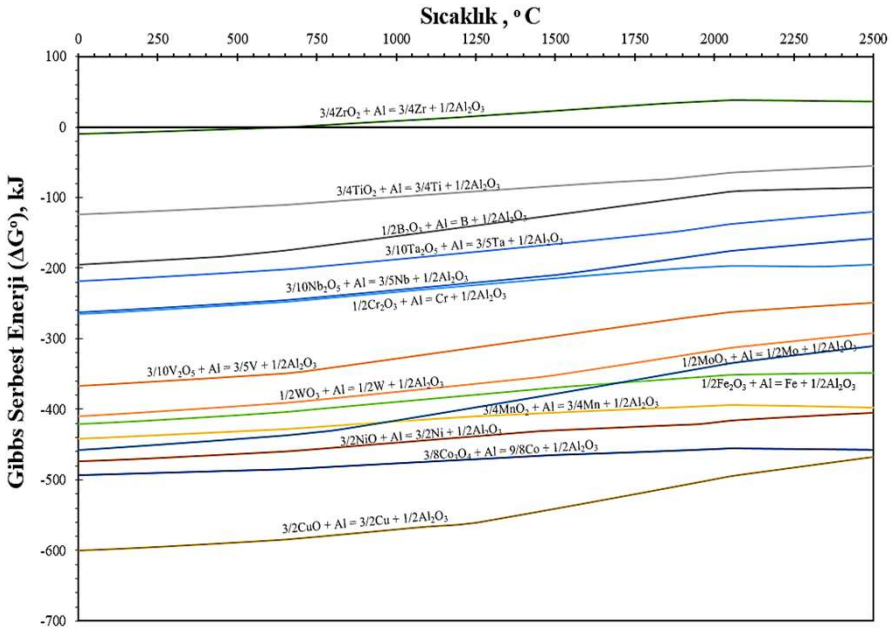

Figure 5.2. Standard free energy changes of reactions of various metal oxides with one mole of Al (HSC 6.2, 2007)

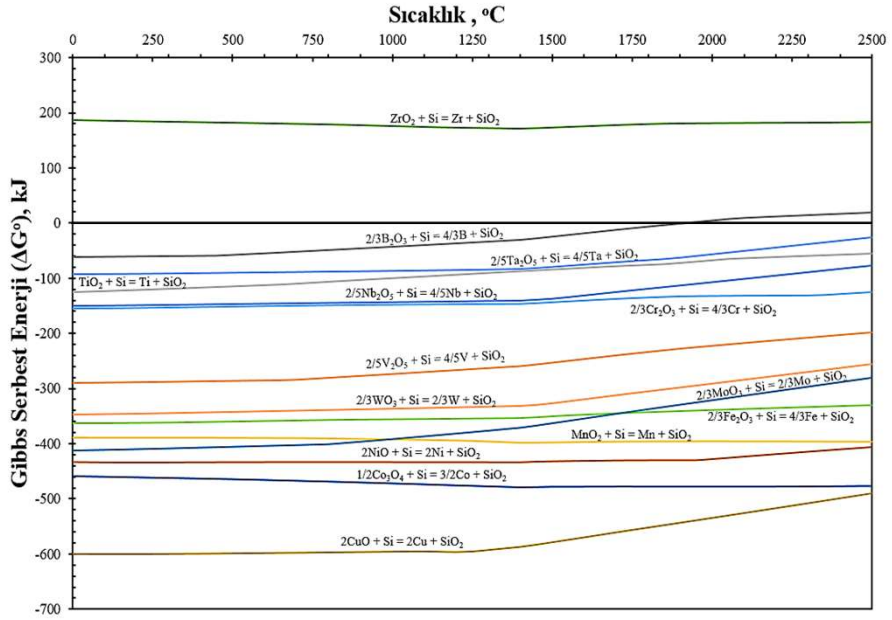

Figure 5.3. Standard free energy changes of reactions of various metal oxides with one mole of Si (HSC 6.2, 2007)

Figure 5.2 shows that the reduction reactions of metal oxides, except ZrO_2, with Al, have negative free energy changes. ZrO_2 can be reduced at lower temperatures than 500 °C. The reduction tendency of metal oxides with Al is from high to low in the following order: CuO, Co_3O_4, NiO, MoO_3, MnO_2, Fe_2O_3, WO_3, V_2O_5, Cr_2O_3,

Nb_2O_5, Ta_2O_5, B_2O_3, TiO_2, ZrO_2. According to Figure 5.3, ZrO_2 can not be reduced by silicon, and B_2O_3 can only be reduced below 1900 °C. Considering the reduction tendencies of metal oxides with Si, similar behavior is observed with the reduction tendency with Al. Only the order of TiO_2, Ta_2O_5, and B_2O_3 is changed.

5.2 Result of SHS Experiments

Mo, Nb, Ta, V, and W elements were chosen as the fourth and fifth elements in the $CrFeNiME_IME_{II}$ alloy system. 10 experiments were performed with combinations of ME_I/ME_{II} elements (Mo, Nb, Ta, V, W). However, within the scope of this thesis, four alloy systems were examined. These alloy systems are CrFeNiMoNb, CrFeNiTaMo, CrFeNiNbV and CrFeNiVW. Table 5.1 gives theoretical released energies and adiabatic temperatures of SHS reactions. According to Equation (2.8), adiabatic temperature and released energy values are suitable for controlled production.

Table 5.1 Enthalpy, released energy, and adiabatic temperature values of the reactions for the targetted SHS alloys (HSC 6.2, 2007)

Alloy System	ΔH°rxn,298K (kJ)	Released Energy (J/g)	Tad (°C)
CrFeNiMoNb	-2094.9	3141.8	2791.4
CrFeNiTaMo	-2021.7	2676.8	2726.9
CrFeNiNbV	-1801.2	2971.3	2500.4
CrFeNiVW	-2170.9	3046.8	2919.3

After the thermodynamic analysis was completed, mass calculations were made for CrFeNiMoNb, CrFeNiTaMo, CrFeNiNbV, and CrFeNiVW high entropy alloy systems. The weights of the raw materials in the starting mixtures are given in Table 5.2 based on the calculations. All experimental work was accomplished after thermodynamic analysis and mass calculations. The weight of the starting mixtures was fixed as 150g.

After completing the SHS experiments, the alloys and slags were weighted. The amount of loss was calculated by subtracting the alloy and slag weights from the initial weight. The amounts of the products are given in Table 5.3. The weight of the alloy and slag formed during the production of CrFeNiMoNb and CrFeNiNbV alloys

was found to be more than the initial weight of 150 grams. The reason for the excess weight is that the resistance wire used for initiation melts and enters the structure of the products.

Table 5.2 Amount of raw materials used in SHS experiments

Input (g)	Alloy Systems			
	CrFeNiMoNb	**CrFeNiTaMo**	**CrFeNiNbV**	**CrFeNiVW**
Fe_2O_3	14.62	12.90	16.31	13.67
NiO	16.97	14.98	18.70	15.87
Cr_2O_3	17.27	15.24	19.03	16.14
MoO_3	32.71	28.86		
Nb_2O_5	30.20		33.28	
Ta_2O_5		44.30		
V_2O_5			22.77	19.32
WO_3				49.25
Al	29.12	25.69	30.40	27.23
Si	6.65	5.87	6.94	6.22
Fe	2.46	2.17	2.57	2.30
Total (g)	150.00	150.00	150.00	150.00

Table 5.3 The amount of metal, slag, and loss material obtained as a result of SHS experiments for target HEAs.

Target Alloy System	**Alloy Weight (g)**	**Slag Weight (g)**	**Loss Weight (g)**
CrFeNiMoNb	62.41	87.76	
CrFeNiTaMo	45.40	97.61	6.99
CrFeNiNbV	55.15	96.81	
CrFeNiVW	69.76	77.60	2.64

The chemical compositions of the obtained slag and alloys were determined by XRF analysis. According to these results, the entropy values of the alloy systems were calculated. The entropy value of the CrFeNiNbV alloy system is 1.83R, and the entropy value of the CrFeNiMoNb alloy system is 1.53R. However, the CrFeNiVW and CrFeNiTaMo alloy systems have an entropy of 1.16R and 1.42R, respectively. CrFeNiNbV and CrFeNiMoNb systems are in the high entropy alloy group since their entropy values are higher than 1.5R.

By using the weights of the final product and the chemical compositions, the distributions of the elements on the products were calculated according to Equation (5.1). $[D_{Me}]$ is the dispersion ratio of metal in the alloy.

$$[D_{Me}] \text{ or } (D_{Me}) = \frac{[\%Me]x \text{ Weight of alloy or } (\%Me)x \text{ Weight of slag}}{wt.\% \text{ Me İn initial mix x weight of initial mix}} \quad (5.1)$$

5.2.1 CrFeNiMoNb Alloy System

The metal distributions on alloy, slag, and scattered part for CrFeNiNbV alloy were given in Figure 5.4. The metal recovery values were calculated as: 90.9% Fe, 82.8% Mo, 79.6% Ni, 55.9% Nb, and 44.3% Cr, respectively.

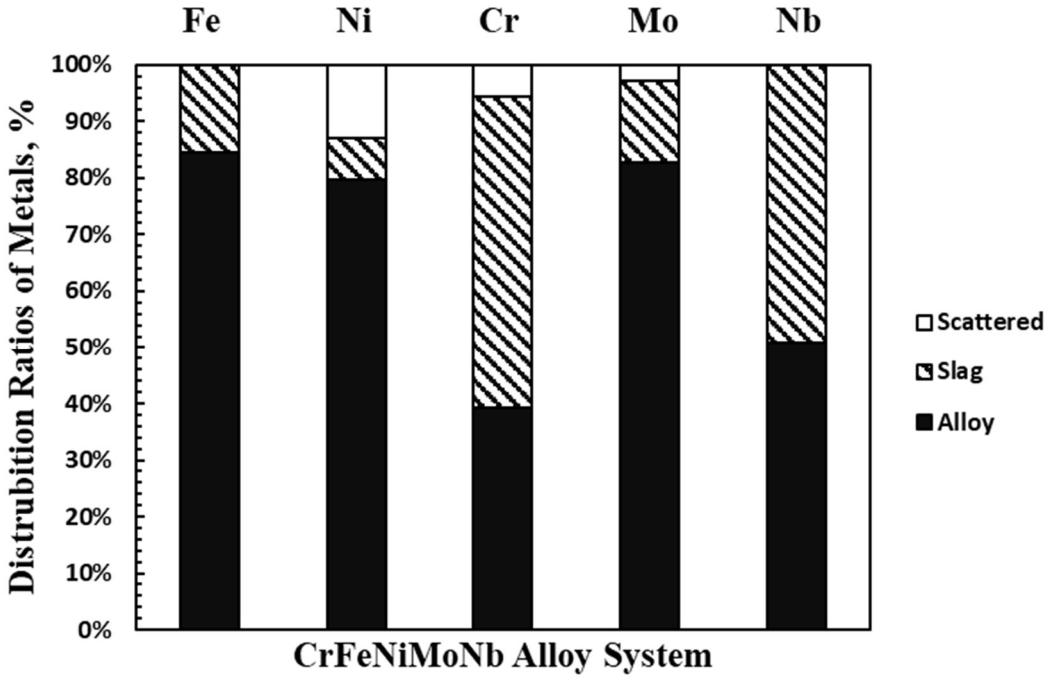

Figure 5.4 The distribution ratios of each element on SHS products for CrFeNiMoNb alloy

The back-scattered electron image of CrFeNiMoNb alloy with the selected areas is given in Figure 5.4. By considering the contrast difference, there were at least three phases in the alloy. There were dendritic and interdendritic structures in the microstructure. In order to determine the phases in the microstructure, it was necessary to evaluate the EDS results from the regional analyzes and the values calculated with the Thermo-Calc software. The chemical compositions of the selected areas in Figure 5.5 are given in Table 5.4.

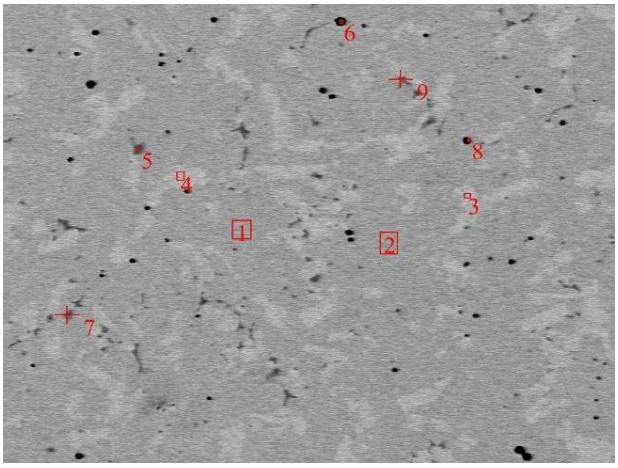

Figure 5.5 The back-scattered electron (BSE) images of estimated CrFeNiMoNb alloy

For the CrFeNiMoNb alloy, regional analysis (EDS) was performed in 9 different areas. It has been observed that the Al content is very high in the regions marked with 7 and 9, and these regions are thought to belong to the slag residues trapped in the metal. Mo-riched and Nb-riched phases were observed in dendrites (regions 1 and 2). Interdendrites (regions 3 and 4) were also rich in refractory metals.

Table 5.4 Chemical compositions (wt.%) of CrFeNiMoNb R-YEA as measured by SEM/EDS technique.

Area	**1**	**2**	**3**	**4**	**5**	**6**	**7**	**8**	**9**
Fe	18.68	18.35	14.45	14.49	14.35	14.57	9.28	14.90	7.47
Cr	8.63	8.40	7.37	7.38	7.15	6.80	4.41	7.41	3.12
Mo	21.73	20.05	27.69	29.88	15.84	15.93	10.16	18.69	7.99
Nb	19.53	21.93	15.74	16.15	13.28	17.87	7.62	13.03	5.88
Si	0.11	0.16	0.59	0.22	0.01	0.00	0.00	0.52	0.01
Al	4.93	4.70	14.92	12.84	24.05	22.71	44.91	22.48	42.37
Ni	7.62	9.78	5.62	6.69	3.88	8.93	2.42	4.43	1.56

The result of the XRD analysis for CrFeNiMoNb alloy is given in Figure 5.6, and five phases were observed in the microstructure. These phases were determined as MoNi, Fe_2Nb, $Cr_9Mo_{21}Ni_{20}$, $Fe_{0.2}Nb_{0.8}$, and $NbNi_3$. A cooling graph obtained by Thermo-Calc software was examined. According to Thermo-Calc calculation, the structural design of these phases was C14 Laves, NI3TA_D0A, MU_Phase, and SIGMA.

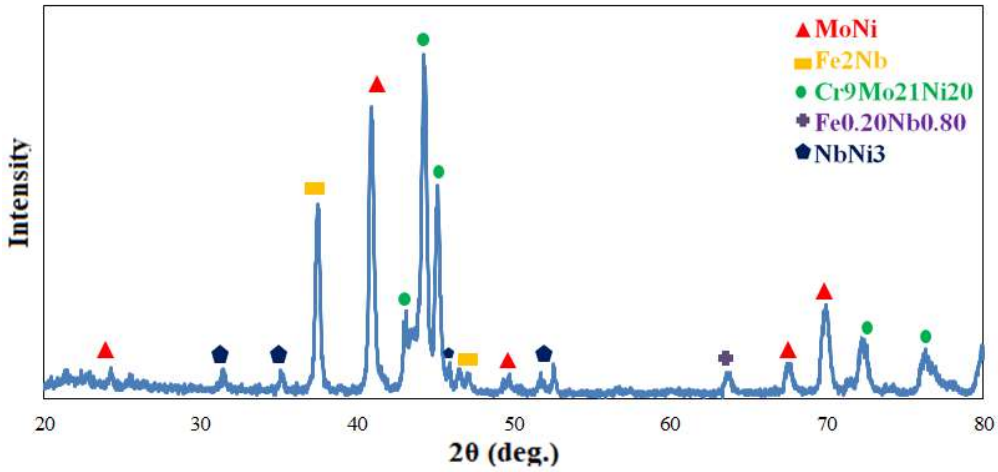

Figure 5.6 XRD results of CrFeNiMoNb alloy system

5.2.2 CrFeNiTaMo Alloy System

The metal distributions on SHS products for CrFeNiTaMo alloy are given in Figure 5.7. The obtained metal recovery values were 52.4% Cr, 92.8% Fe and 73.7% Ni, respectively. The metal recoveries for refractory metals were also measured as: 68.9% Mo and 12.1% Ta, respectively. Since the enthalpy of the reaction equals -2021.7 kJ and the reduction potential of tantalum oxide with Al and Si is lower than that of other metal oxides, it is thought that the Ta recovery efficiency remains low.

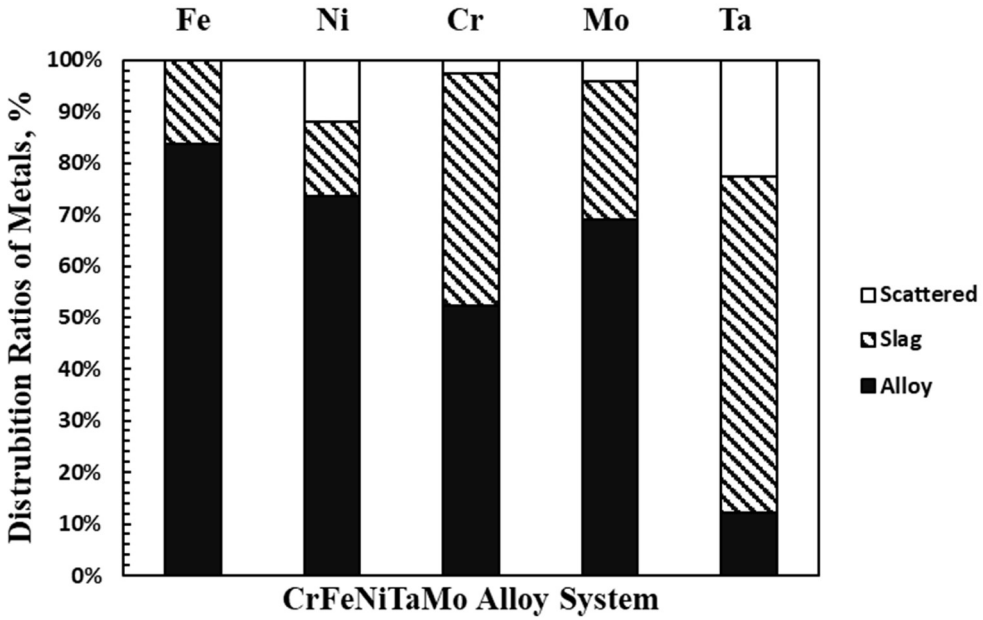

Figure 5.7 The distribution ratios of each element on SHS products for CrFeNiTaMo alloy

There are at least three phases with different contrast in the CrFeNiTaMo alloy system, and a dendritic solidification has been observed in Figure 5.8. The presence of different phases was observed between dendrites. In order to determine the phases in the microstructure, regional analyzes were made in 9 different areas with EDS analysis.

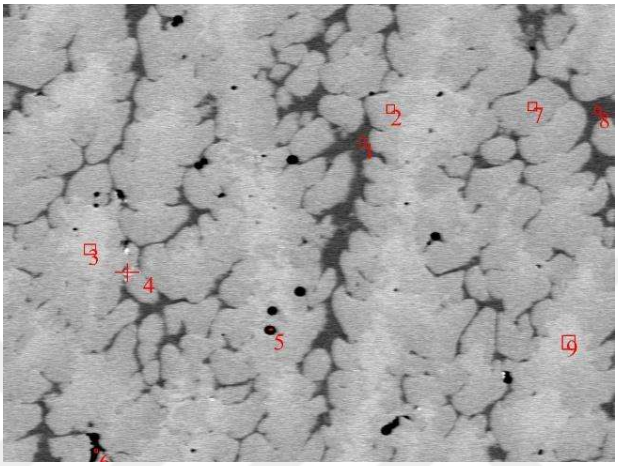

Figure 5.8 The back-scattered electron (BSE) images of estimated CrFeNiTaMo alloy

In the analysis results made with the EDS technique given in Table 5.5, it is seen that Ta is much lower than the target composition and reduced at a lower rate than other transition elements. Due to rapid solidification, there are shrinkage gaps in the alloy structure. In these areas (regions 5 and 6), the amount of Al is high, and other elements could not be reduced. There were Mo-riched structures in the center of the dendrites (regions 3, 7, and 9) and the dendrite boundary (region 2). Also, atomic compositions of Cr, Fe, Ni, and Si were over 10%. Between the dendrites (regions 1 and 8), there was a structure with high compositions of Ni, Fe, and Cr, and the amount of Mo element was decreased.

The result of the XRD analysis for CrFeNiTaMo alloy is given in Figure 5.9. A cooling graph obtained by Thermo-Calc software was examined, and four phases were observed in the microstructure. These phases were determined as MoCr, Fe_2Ta, Ni_2Ta, and $Cr_5Mo_{11}Ni_{11}$. According to Thermo-Calc calculation, the structural designs of these phases were C14 Laves, MU_Phase, NI2TA_C11B, and SIGMA.

Table 5.5 Chemical compositions (wt.%) of CrFeNiTaMo R-YEA as measured by SEM/EDS technique.

Area	1	2	3	4	5	6	7	8	9
Fe	28.77	18.71	19.37	7.24	8.62	6.08	19.26	28.90	19.66
Cr	18.24	11.23	10.92	11.39	10.23	4.67	12.21	18.42	11.08
Si	5.52	18.07	16.99	0.00	3.60	2.67	16.30	3.71	16.73
Al	6.17	0.47	0.50	1.38	39.80	71.88	0.32	7.33	0.75
Mo	5.11	26.77	24.44	13.04	9.70	6.59	27.81	3.80	24.11
Ni	33.05	13.93	13.55	6.79	8.36	4.03	14.72	35.07	13.19
Ta	1.99	9.95	13.98	59.68	3.06	2.96	8.25	1.32	14.10

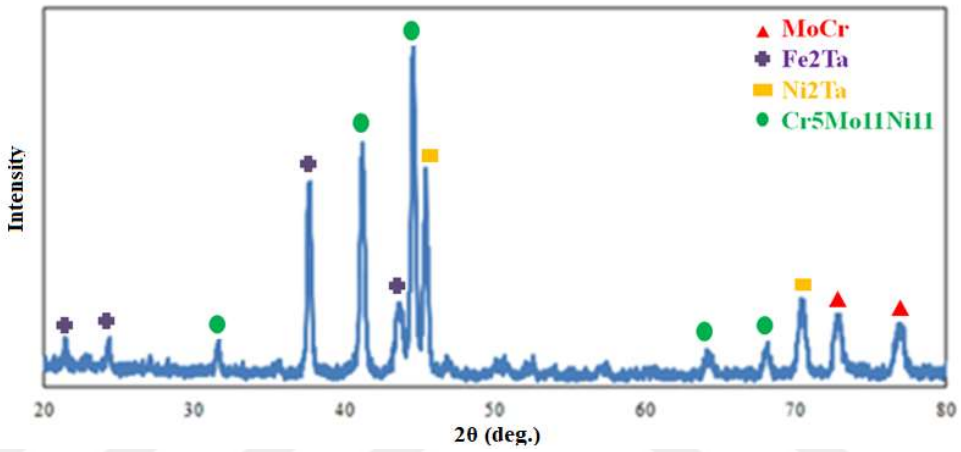

Figure 5.9 XRD results of CrFeNiTaMo alloy system

5.2.3 CrFeNiNbV Alloy System

The metal distributions on alloy, slag and scattered part for CrFeNiNbV alloy are given in Figure 5.10. The metal recovery values were calculated as: 86.2% Fe, 72.0% Ni, 58.7% Nb, 50.2% Cr, and 40.6% V, respectively.

By looking at the microstructure image given in Figure 5.11, at least three phases with different contrasts in the CrFeNiNbV alloy system and dendritic solidification have been observed. The presence of different phases was observed between dendrites. In order to determine the phases in the microstructure, regional analyzes were made in 7 different areas with EDS analysis. The results of the EDS analysis are given in Table 5.6.

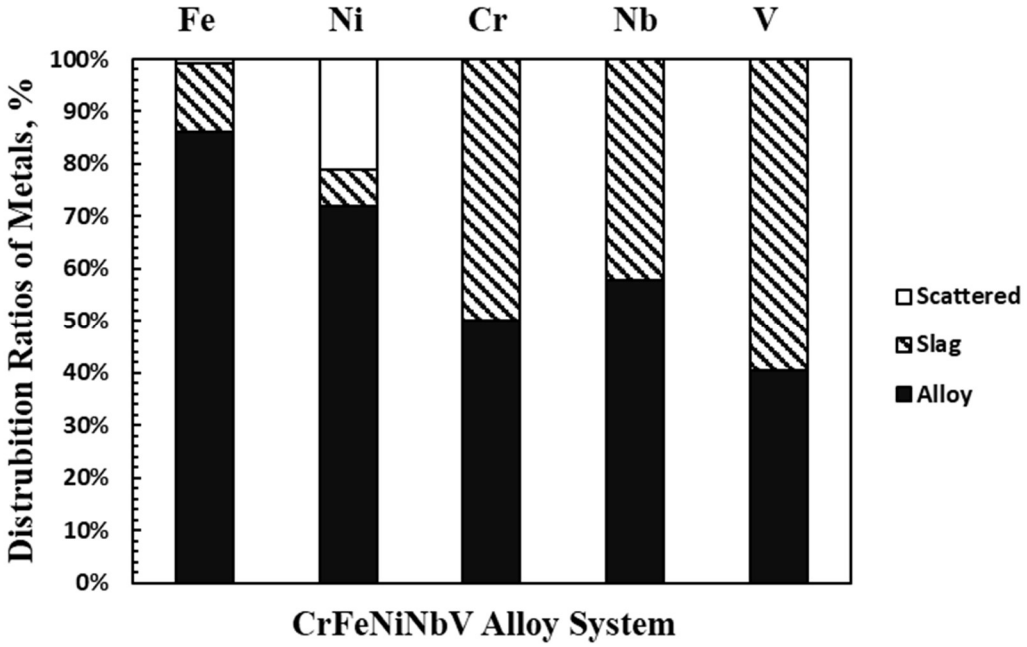

Figure 5.10 The distribution ratios of each element on SHS products for CrFeNiNbV alloy.

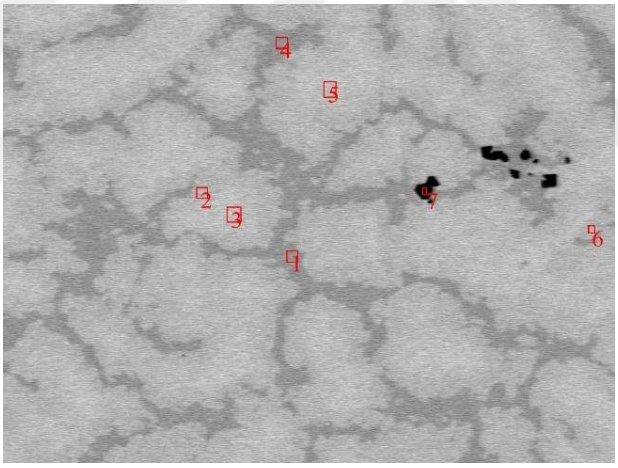

Figure 5.11 SEM image of CrFeNiNbV R-YEA showing the EDS regions at 1000 magnification.

Table 5.6 Chemical compositions (wt.%) of CrFeNiNbV R-YEA as measured by SEM/EDS technique.

Area	1	2	3	4	5	6	7
Si	4.41	12.80	13.97	5.14	14.78	12.01	4.20
Al	5.50	0.41	0.42	5.49	0.67	1.12	19.27
Cr	17.00	11.56	10.82	17.52	10.36	12.04	13.63
Fe	25.38	19.81	19.21	24.99	18.78	19.78	20.51
Ni	29.51	17.92	14.01	28.80	13.89	20.47	22.73
Nb	3.12	28.00	35.03	3.71	34.88	23.32	3.92
V	14.39	9.50	6.54	14.30	6.65	10.36	11.63

By considering the region analyses given in Table 5.6, it is seen that some phases in the microstructure were riched in refractory metals, and some were not. Dendritic solidification was observed in the microstructure of the CrFeNiNbV alloy. In addition, there were micro-segregations within the dendrite.

There was a Nb-riched structure in the center of the dendrites (regions 3 and 5). In this structure, there were also Cr, Fe, Ni, and Si, whose atomic composition is over 10%. At the dendrite boundary (regions 2 and 6), the Nb composition decreased slightly, while the Ni and V compositions increased. Between the dendrites (regions 1 and 4), there was a structure with high Ni, Fe, Cr, and V compositions.

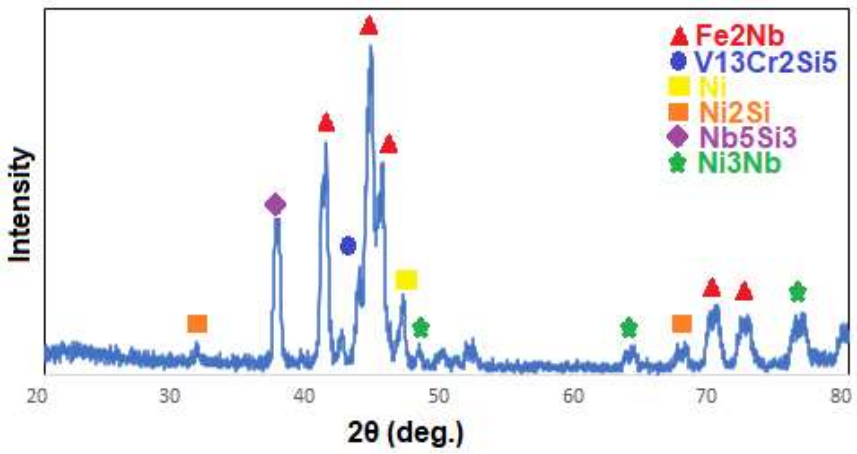

Figure 5.12 XRD results of CrFeNiNbV alloy system

The result of the XRD analysis for CrFeNiNbV alloy is given in Figure 5.12. A cooling graph obtained by Thermo-Calc software was examined, and six phases were observed in the microstructure.

According to XRD analysis, these phases were determined as Fe_2Nb, Ni, $V_{13}Cr_2Si_5$, Ni_2Si, Nb_5Si_3, and Ni_3Nb. The C14 Laves phase was specified as Fe_2Nb. Si-containing phases were observed in the alloy system because ferrosilicon was used as the reducing agent. The structural design of these phases was A15, C14 Laves, MU_Phase, NI31SI12, D0A, and D8l.

5.2.4 CrFeNiVW Alloy System

The metal distributions on alloy, slag, and scattered part for CrFeNiVW alloy were given in Figure 5.13. The metal recovery values were calculated as: 99.2% Fe, 84.1% Ni, 82.4% W, 61.4% Cr, and 42.6% V, respectively.

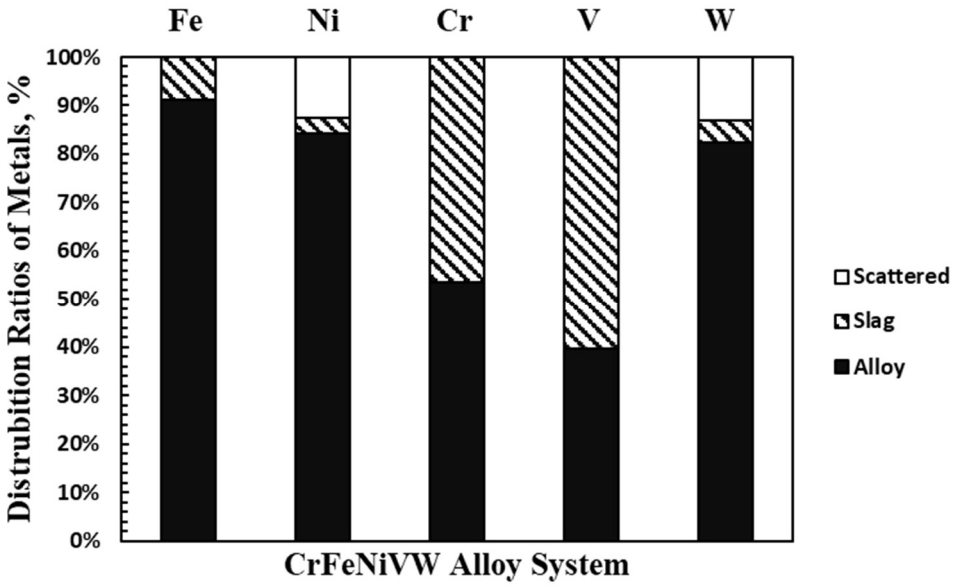

Figure 5.13 The distribution ratios of each element on SHS products for CrFeNiVW alloy

The SEM image for the CrFeNiVW alloy system is given in Figure 5.14. There were at least four phases with different contrast in the microstructure. Phases with different grain sizes were observed in the microstructure. It has been predicted that peritectic transformation may occur in light-colored regions based on the contrast difference. Elements with high melting points (V, W) will solidify earlier than other elements. Therefore these regions are expected to be rich in V and W elements. In order to determine the phases in the microstructure, regional analyzes were made in 10 different areas with EDS analysis.

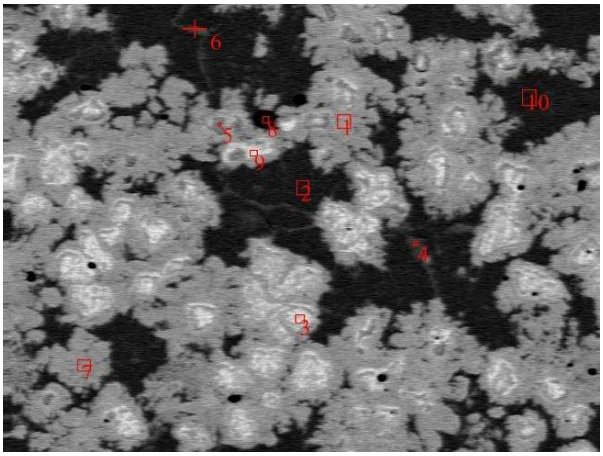

Figure 5.14 The back-scattered electron (BSE) images of estimated CrFeNiVW alloy

The results of the EDS analysis of the estimated CrFeNiVW alloy are given in Table 5.7. There was a Fe-riched and W-riched structure in the center of the dendrites (regions 1 and 7). Also, the atomic compositions of Cr and Si were over 10%. Between the dendrites (regions 2 and 10), there was a structure with high compositions of Ni and Fe. The W content is high in the first solidified phases from the molten state, so the W content is higher in the light-colored regions (3 and 9) and at very low levels in the inter-dendrites regions.The fact that the V element is in the alloy at a lower rate than expected confirms the distribution ratios on the product.

Table 5.7 Chemical compositions (wt.%) of CrFeNiVW R-YEA as measured by SEM/EDS technique.

Area	**1**	**2**	**3**	**4**	**5**	**6**	**7**	**8**	**9**	**10**
Fe	23.14	26.38	2.98	21.89	4.21	22.24	23.69	3.11	6.07	26.03
Cr	13.70	10.61	2.68	15.43	3.37	16.30	13.51	1.59	5.56	11.49
Al	0.50	7.08	1.62	1.01	0.13	1.05	0.74	66.82	0.61	7.33
Ni	13.43	37.62	2.44	26.60	3.37	23.00	15.19	3.88	4.86	36.94
Si	6.46	8.96	0.00	14.89	0.00	12.53	7.02	0.66	0.00	7.88
W	33.78	1.32	79.53	6.53	67.73	10.06	30.46	1.19	73.56	1.57
V	8.27	7.66	3.19	13.46	3.46	14.02	8.84	1.14	4.21	7.66

The result of the XRD analysis for CrFeNiVW alloy was given in Figure 5.15. Five phases were observed in the microstructure. According to XRD analysis, these phases were determined as Cr_3Ni_2, W, FeV, FeNi, and Fe_7W_6. The C14 Laves phase was specified as Fe2Nb. The structural design of these phases was BCC_B2, FCC_L12, and SIGMA.

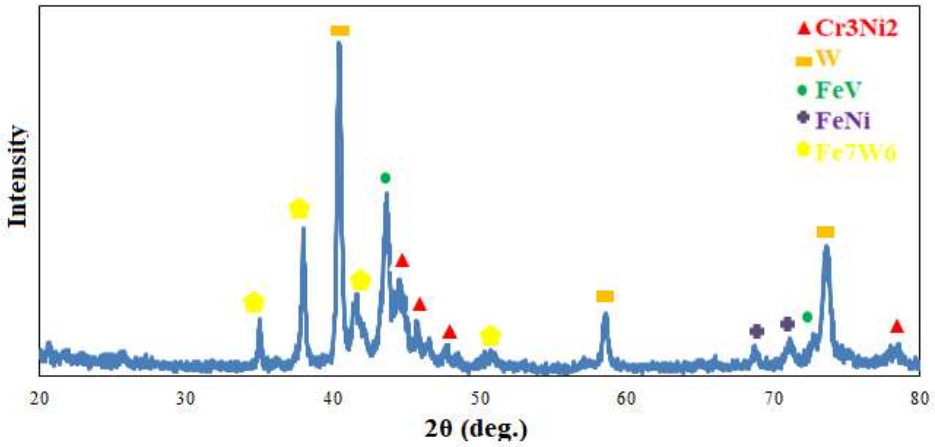

Figure 5.15 XRD results of CrFeNiVW alloy system

5.2.5 Analysis of the Microhardness for Alloy Systems

Five Vickers hardness values were measured for CrFeNiMoNb, CrFeNiTaMo, CrFeNiNbV, and CrFeNiVW alloy systems. The average of these values was taken, and the standard deviation values were calculated. The microhardness graph of the measurements is given in Figure 5.16, and the average microhardness values are given in Table 5.8.

Table 5.8 Average microhardness values of alloys ($HV_{0.3}$)

Targetted Alloy System	**HV (Vickers Hardness)**					**Average HV**	**Standard Deviation**
	1	2	3	4	5		
CrFeNiMoNb	980	968	980	993	964	977.0	10.24
CrFeNiTaMo	979	875	940	959	972	945.0	37.43
CrFeNiNbV	1032	1051	1050	1040	1046	1043.8	7.05
CrFeNiVW	943	900	951	916	964	934.8	23.44

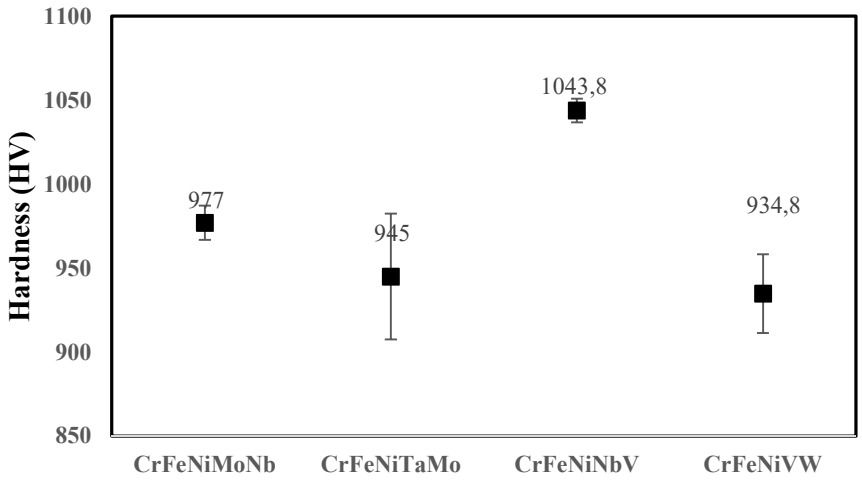

Figure 5.16 Microhardness of R-HEAs obtained after SHS experiments

When the hardness values of the alloys are compared, the CrFeNiNbV alloy has the highest average hardness value. The high hardness value is due to the presence of Laves phase in the microstructure. CrFeNiMoNb, CrFeNiTaMo, and CrFeNiVW alloys have the average hardness values of 977, 945, and 934 HV, respectively. The lowest hardness in the alloy systems produced was observed in the CrFeNiVW alloy. However, all alloy systems have higher hardness compared to conventional alloys.

CHAPTER 6
CONCLUSIONS

Overall conclusions of this thesis, based on the results of the experiments obtained, are as follows:

1. In this thesis, the production of high entropy alloys containing refractory metals $CrFeNiME_IME_{II}$ was carried out using the self-propagating high-temperature synthesis (SHS) method. Equiatomic alloy compositions were targeted for CrFeNiMoNb, CrFeNiTaMo, CrFeNiNbV, and CrFeNiVW systems.

2. The mixtures of metal oxide powders (Fe_2O_3, Cr_2O_3, NiO, MoO_3, V_2O_5, Nb_2O_5, WO_3, Ta_2O_5) were used as raw materials. Aluminum and ferrosilicon powders were used as reducing agents. The reducing mixture was prepared so that 75% of the reductant amount came from Al and 25% from ferrosilicon.

3. The specific heat and adiabatic temperature values used in the SHS method were calculated theoretically. Suitable energy values were obtained, and SHS experiments were carried out under atmospheric conditions.

4. The final products were characterized using XRF, XRD, SEM/EDS, and hardness tests.

5. XRF analysis of the slags showed that there was some metal leakage into the slags because of the rapid solidification.

6. The distributions of the elements and metal recovery efficiencies were realized. Among refractory metals, the highest metal recovery was obtained in W, and the lowest was observed in Ta.

7. The entropy values of the alloy systems were calculated depending on the chemical analysis. The entropy value of the CrFeNiNbV alloy system was 1.83R,

and the entropy value of the CrFeNiMoNb alloy system was 1.53R. However, the CrFeNiVW and CrFeNiTaMo alloy systems have an entropy of 1.16R and 1.42R, respectively. CrFeNiNbV and CrFeNiMoNb systems were in the high entropy alloy group since their entropy values were higher than 1.5R.

8. The cooling graphs were obtained by Thermo-Calc software, and the results were compared with XRD analysis. According to the XRD results, all alloy systems had at least four phases. CrFeNiMoNb, CrFeNiTaMo, CrFeNiNb, and CrFeNiVW alloy systems all have a C14 Laves phase resulting from rapid cooling.

9. The cooling graphs obtained by Thermo-Calc software and the results obtained from XRD analysis were compatible, the phases which were observed in cooling graphs were obtained with XRD analysis. It was observed that there are mostly MU_PHASE and SIGMA phases in the structure.

10. According to SEM/EDS analysis, there were dendritic and interdendritic structures in the CrFeNiMoNb alloy. Dendritic solidification was observed for CrFeNiTaMo and CrFeNiNbV alloy. Peritectic transformation may have occurred in the CrFeNiVW alloy system. Also, phases with different grain sizes were observed in the microstructures.

11. CrFeNiNbV alloy has the highest hardness value. The high hardness value is due to the presence of Laves phase in the microstructure. The lowest hardness in the alloy systems produced was observed in the CrFeNiVW alloy. However, all alloy systems have higher hardness compared to conventional alloys.

12. The efficiency of Ta element is lower than other metals since the enthalpy of the reaction equals -2021.7 kJ and the reduction potential of tantalum oxide with Al and Si is lower than that of other metal oxides. Besides the amount of Ta is much lower than the target composition in the structure and there are hollow structures in the alloy due to the rapid solidification.

13. The alloy system containing W (CrFeNiVW) has the lowest hardness value, according to the SEM/EDS and XRF analyses, the amount of W is much less than expected in some regions. This is because of the lack of reduction of WO_3.

REFERENCES

Alkan, M. (2014). *Kendiliğinden ilerleyen yüksek sıcaklık sentezi yöntemi ile yeni ve özel alaşımların üretimi ve geliştirilmesi* [Doctoral dissertation]. İstanbul Teknik Üniversitesi, İstanbul.

Bizhanova, G., Li, F., Ma, Y., Gong, P., & Wang, X. (2018). Development and crystallization kinetics of novel near-equiatomic high-entropy bulk metallic glasses. *Journal of Alloys and Compounds*, *779*, 474–486. https://doi.org/10.1016/j.jallcom.2018.11.299

Borovinskaya, I. P. (1992). Chemical classes of the SHS processes and materials. *Pure and Applied Chemistry*, *64*(7), 919–940. https://doi.org/10.1351/pac199264070919

Cheng, C. Y., Yang, Y. C., Zhong, Y. Z., Chen, Y. Y., Hsu, T., & Yeh, J. W. (2017). Physical metallurgy of concentrated solid solutions from low-entropy to high-entropy alloys. *Current Opinion in Solid State and Materials Science*, *21*(6), 299–311. https://doi.org/10.1016/j.cossms.2017.09.002

Chikumba, S., & Rao, V. V. (2015). High entropy alloys: Development and applications. *7th International Conference on Latest Trends in Engineering and Technology (ICLTET'2015) Nov. 26-27, 2015 Irene, Pretoria (South Africa),* 13–17. https://doi.org/10.15242/IIE.E1115005

Crider, J. F. (1982). Self-propagating high temperature synthesis–-A Soviet method for producing ceramic materials. *Ceramic Engineering and Science Proceedings*, 519–528. https://doi.org/10.1002/9780470318782.ch8

Cui, P., Ma, Y., Zhang, L., Zhang, M., Fan, J., Dong, W., Yu, P., Li, G., & Liu, R. (2018). Effect of Ti on microstructures and mechanical properties of high entropy alloys based on CoFeMnNi system. *Materials Science and Engineering*: A, *737*, 198–204. https://doi.org/10.1016/j.msea.2018.09.050

Davis, J. R. (1990). Properties and selections : Irons, steels and high performance alloys. In *ASM Handbook* (Vol. 1).

Feng, R., Gao, M., Lee, C., Mathes, M., Zuo, T., Chen, S., Hawk, J., Zhang, Y., & Liaw, P. (2016). Design of light-weight high-entropy alloys. *Entropy*, *18*(9), 333. https://doi.org/10.3390/e18090333

Gao, X. Q., Zhao, K., Ke, H. B., Ding, D. W., Wang, W. H., & Bai, H. Y. (2011). High mixing entropy bulk metallic glasses. *Journal of Non-Crystalline Solids*, *357*(21), 3557–3560. https://doi.org/10.1016/j.jnoncrysol.2011.07.016

Greven, A., Keller, G., & Warnecke, G. (2003). *Entropy*.

Kang, B., Kong, T., Ryu, H. J., & Hong, S. H. (2021). Superior mechanical properties and strengthening mechanisms of lightweight AlxCrNbVMo refractory high-entropy alloys (x = 0, 0.5, 1.0) fabricated by the powder metallurgy process. *Journal of Materials Science and Technology*, *69*, 32–41. https://doi.org/10.1016/j.jmst.2020.07.012

Levashov E.A., Padyukov K.L. (1993). *Self-propagating high-temperature synthesis: a new method for production of diamond-containing materials*. Diam Relat Mater, *2*, 207-210.

Li, R., Gao, J., & Fa, K. (2010). Study to microstructure and mechanical properties of Mg containing high entropy alloys. *Materials Science Forum*, *650*, 265–271. https://doi.org/10.4028/www.scientific.net/MSF.650.265

Li, W., Xie, D., Li, D., Zhang, Y., Gao, Y., & Liaw, P. K. (2021). Mechanical behavior of high-entropy alloys. *Progress in Materials Science*, *118*, 1–142. https://doi.org/10.1016/j.pmatsci.2021.100777

Li, Y., Wang, S., Wang, X., Yin, M., & Zhang, W. (2020). New FeNiCrMo(P, C, B) high-entropy bulk metallic glasses with unusual thermal stability and corrosion resistance. *Journal of Materials Science and Technology*, *43*, 32–39. https://doi.org/10.1016/j.jmst.2020.01.020

Liu, W. H., He, J. Y., Huang, H. L., Wang, H., Lu, Z. P., & Liu, C. T. (2015). Effects of Nb additions on the microstructure and mechanical property of CoCrFeNi high-entropy alloys. *Intermetallics*, *60*, 1–8. https://doi.org/10.1016/j.intermet.2015.01.004

Merzhanov, A. G. (1995). History and recent developments in SHS. *Ceramics International*, *21*(5), 371–379. https://doi.org/10.1016/0272-8842(95)96211-7

Merzhanov, Alexander G. (2012). 40 years of SHS: A lucky star of a scientific discovery. In *Bentham e-Books*.

Mishra, S. K., & Pathak, L. C. (2009). Self-propagating high-temperature synthesis (SHS) of advanced high-temperature ceramics. *Key Engineering Materials*, *395*, 15–38. https://doi.org/10.4028/www.scientific.net/kem.395.15

Munitz, A., Kaufman, M. J., Nahmany, M., Derimow, N., & Abbaschian, R. (2018). Microstructure and mechanical properties of heat treated Al1.25CoCrCuFeNi high entropy alloys. *Materials Science and Engineering: A*, *714*, 146–159. https://doi.org/10.1016/j.msea.2017.12.084

Murty, B. S., Ranganathan, S., Yeh, J. W., & Bhattacharjee, P. P. (2019). High-entropy alloys. In *High-Entropy Alloys*. https://doi.org/10.1016/C2017-0-03317-7

Murty, B. S., Yeh, J. W., Ranganathan, S., & Bhattacharjee, P. P. (2019). Chapter 1-A brief history of alloys and the birth of high-entropy alloys. In *High-Entropy Alloys*, 1–12. Elsevier. https://doi.org/10.1016/B978-0-12-816067-1.00001-1

Pacheco, M. M. (2007). *Self-sustained high-temperature reactions: Initiation, propagation and synthesis*. Strategic Research Program of the Netherlands Institute for Metals Research, Netherlands.

Saikumaran, A., Jaiganesh, Ghosh, C., Mythili, R., Sornadurai, D., Subramanian, N., Jaya, S. M., & Saibaba, S. (2019). Experimental and theoretical study of microstructural characteristics and phase stability in equiatomic CrFeMoV alloy. *Materials Characterization*, *154*(June), 449–457. https://doi.org/10.1016/j.matchar.2019.06.027

Saikumaran, A., Mythili, R., Saroja, S., & Srihari, V. (2019). Microstructural characterization of equiatomic CrFeNbNiV alloy. *Transactions of the Indian Institute of Metals*, *72*(1), 111–121. https://doi.org/10.1007/s12666-018-1466-x

Sanin, V. N., Yukhvid, V. I., Ikornikov, D. M., Andreev, D. E., Sachkova, N. V., & Alymov, M. I. (2016). SHS metallurgy of high-entropy transition metal alloys.

Doklady Physical Chemistry, *470*(2), 145–149. https://doi.org/10.1134/S001250161610002X

Senkov, O. N., Wilks, G. B., Miracle, D. B., Chuang, C. P., & Liaw, P. K. (2010). Refractory high-entropy alloys. *Intermetallics, 18*(9)*,* 1758–1765. https://doi.org/10.1016/j.intermet.2010.05.014

Sobol', O. (2020). Structure and properties of high-entropy alloys based on refractory metals. *Materials Today: Proceedings*, *30*, 736–741. https://doi.org/10.1016/j.matpr.2020.01.556

Stepanov, N. D., Shaysultanov, D. G., Chernichenko, R. S., Ikornikov, D. M., Sanin, V. N., & Zherebtsov, S. V. (2018). Mechanical properties of a new high entropy alloy with a duplex ultra-fine grained structure. *Materials Science and Engineering A, 728*, 54–62. https://doi.org/10.1016/j.msea.2018.04.118

Tsai, M.-H. (2016). Three strategies for the design of advanced high-entropy alloys. *Entropy, 18*(7), 252. https://doi.org/10.3390/e18070252

Tseng, K., Yang, Y., Juan, C., Chin, T., Tsai, C., & Yeh, J. (2017). A light-weight high-entropy alloy Al20Be20Fe10Si15Ti35*. Science China Technological Sciences, 61*(2)*,* 184–188. https://doi.org/10.1007/s11431-017-9073-0

Yeh, J. W. (2006). Recent progress in high-entropy alloys. *Annales de Chimie: Science Des Materiaux, 31*(6), 633–648. https://doi.org/10.3166/acsm.31.633-648

Yeh, J. W. (2013). Alloy design strategies and future trends in high-entropy alloys. *The Minerals, Metals & Materials Society, 65*(12), 1759–1771. https://doi.org/10.1007/s11837-013-0761-6

Yeh, J. W. (2015). Physical metallurgy of high-entropy alloys. *The Minerals, Metals & Materials Society, 67*(10), 2254–2261. https://doi.org/10.1007/s11837-015-1583-5

Yeh, J. W. (2016). Chapter 1- Overview of high-entropy alloys. In M. C. Gao, P. K. Liaw, J. W. Yeh, & Y. Zhang (Eds.), *High-entropy alloys: Fundamentals and applications*, 1–19. Springer. https://doi.org/10.1007/978-3-319-27013-5

Zhang, W., Liaw, P. K., & Zhang, Y. (2018). Science and technology in high-entropy alloys. *Science China Materials*, *61*, 1–21. https://doi.org/10.1007/s40843-017-9195-8.

Zhang, Y. (2019*). High-entropy materials-A brief introduction*. Springer Nature Singapore Pte Ltd. https://doi.org/10.1007/978-981-13-8526-1

Zhang, Y., Zuo, T. T., Tang, Z., Gao, M. C., Dahmen, K. A., Liaw, P. K., & Lu, Z. P. (2014). Microstructures and properties of high-entropy alloys. *Progress in Materials Science, 61*, 1–93. https://doi.org/10.1016/j.pmatsci.2013.10.001